# SUPERSONIC EJECTOR-DIFFUSER THEORY AND EXPERIMENTS

A. L. Addy[†]
J. Craig Dutton[††]
C. C. Mikkelsen[†††]

August 1981

Supported by

U.S. Army Research Office
Grant Number DAHC 04-74-G-0112

and

Department of Mechanical and Industrial Engineering
University of Illinois at Urbana-Champaign
Urbana, Illinois 61801

---

[†] Professor and Associate Head, Department of Mechanical and Industrial Engineering, University of Illinois at Urbana-Champaign, Urbana, Illinois.

[††] Assistant Professor, Department of Mechanical Engineering, Texas A&M University, College Station, Texas.

[†††] Aerospace Engineer, U.S. Army MICOM, Redstone Arsenal, Alabama.

TABLE OF CONTENTS

## LIST OF FIGURES

LIST OF TABLES

# NOMENCLATURE

Symbols

| | |
|---|---|
| $A$ | Area |
| $C_1, C_2, C_3$ | Constants defined in text |
| $C_p$ | Specific heat at constant pressure |
| $D$ | Diameter |
| $f( )$ | Function |
| $f_1( ), \ldots, f_5( )$ | Gas dynamic functions defined in text |
| $g, g( )$ | Gravitational acceleration or function |
| $h$ | Specific enthalpy |
| $L$ | Length |
| $M$ | Mach number |
| $Mw$ | Molecular weight |
| $P$ | Pressure |
| $R$ | Gas constant |
| $r_d$ | Diffuser compression coefficient |
| $t$ | Time |
| $V$ | Magnitude of velocity |
| $w$ | Mass flowrate |
| $W_{ss}$ | Work, shaft and shear |
| $X$ | Longitudinal coordinate or flow direction coordinate |
| $Y, Z$ | Coordinates |
| $\gamma$ | Ratio of specific heats |
| $\rho$ | Density |
| $\mu$ | Secondary-to-primary mass flowrate ratio, $w_s/w_p$ |

Subscripts

| | |
|---|---|
| 0 | Stagnation state or location |
| 1,2,3,4 | System locations |
| ATM | Atmosphere |
| B | Back |
| BO | Break-off conditions |
| CS | Control surface |
| M | Mixed |
| MAX | Maximum |
| P | Primary |
| S | Secondary |
| T | Total |
| X,Y | Upstream and downstream normal shock locations |

# 1.0 INTRODUCTION

Supersonic ejector-diffuser systems have many applications both in industrial and advanced, high technology settings. These applications include jet pump compression, thrust augmentation, extraction of a secondary fluid, mixing of two streams, ventilation and air conditioning, etc. Another possible application is to the high energy chemical laser. In chemical laser systems, the flow and lasing zones within the laser cavity are established by the interaction, mixing, and reaction of multiple, two-dimensional, supersonic streams at relatively low absolute static pressure levels. Accompanying the mixing and chemical reactions between these streams, considerable energy is released to the flow which tends, qualitatively, to increase the static pressure, to decrease the stagnation pressure, and to decrease the Mach number of the "mixed" supersonic flow within the laser cavity. At the cavity exit this stream must then be pumped to ambient conditions so that the lasing process can be started and sustained. A supersonic ejector-diffuser system is a prime candidate for the pressure recovery required in this corrosive environment.

The objective of this report[†] is to present the results of an integrated theoretical and experimental investigation of supersonic ejector-diffuser systems. In all cases, consideration is limited to configurations for which the primary stream enters the mixing tube supersonically

---

[†]Supported by Army Research Office, DAHC 04-74-G-0112, and the Department of Mechanical and Industrial Engineering.

while the secondary enters subsonically or sonically. The theoretical phase of the investigation emphasizes the development of simplified flow models and computer programs to describe the performance of constant-pressure, constant-area, and staged ejectors. In the experimental investigation, small-scale, cold-flow studies were carried out to obtain quantitative performance data for potential ejector-diffuser configurations. These configurations included various nozzle, mixing-tube, and diffuser geometries which were operated over a range of flow variables. These data serve as a basis for comparison with the theoretical flow models.

The results of this investigation are treated in detail in subsequent sections.

## 2.0 THEORETICAL INVESTIGATION

Four areas are considered in this section; they are:

(1) Supersonic ejector system characteristics;

(2) The constant-pressure ejector;

(3) The constant-area ejector;

(4) The staged ejector.

The discussion of ejector characteristics is qualitative in nature while detailed analyses and discussions are included for each of the last three areas. In addition, the computer programs developed for making the calculations are described; detailed program listings and sample input/output data are included; and representative cases are presented and discussed. The representative cases are not intended to be comprehensive in nature but rather are presented to demonstrate the capabilities, limitations, and the various facets of the simplified theoretical models.

The computer programs have been written with both straightforward subsystems calculations and overall systems studies in mind. It is therefore felt that they can be effectively incorporated into codes developed for preliminary overall systems studies.

### 2.1 SUPERSONIC EJECTOR SYSTEM CHARACTERISTICS

To establish a basis for the detailed modeling and performance analysis of supersonic ejector systems, a qualitative discussion of the performance and nature of such systems is given in this section. Emphasis has been placed on defining the general functional relationships

describing the performance of these systems and how their form is dependent on the internal flow phenomena.

A representative ejector configuration and the associated notation are shown in Fig. 2.1-1. The primary stream is assumed to be supplied from the stagnation state ($P_{P0}$,$T_{P0}$) through a supersonic nozzle and the secondary stream is supplied from the stagnation state ($P_{S0}$,$T_{S0}$). The secondary and primary streams begin their mutual interaction at their point of confluence at the primary nozzle exit. This interaction, as well as the mixing between the streams, continues to the shroud exit where they are discharged to the ambient pressure level $P_{ATM}$.

2.1.1 Performance characteristics

The objective of any ejector analysis is to establish, for a given configuration and working media, the performance characteristics of the system. In general, the mass flow characteristics can be represented functionally by:

$$W_S/W_P = f(P_{S0}/P_{P0}, P_{ATM}/P_{P0}) \quad , \qquad (2.1\text{-}1)$$

i.e., they are dependent on the stagnation pressure and back pressure ratios.

An alternate formulation of the pumping characteristics in terms of the initial secondary stream Mach number, $M_{S1}$, the static pressure ratio $P_{S1}/P_{P0}$ of the secondary stream at the point of confluence of the two streams, and the ambient pressure ratio, $P_{ATM}/P_{P0}$, is given in functional form by:

$$M_{S1} = f(P_{S1}/P_{P0}, P_{ATM}/P_{P0}) \quad . \qquad (2.1\text{-}2)$$

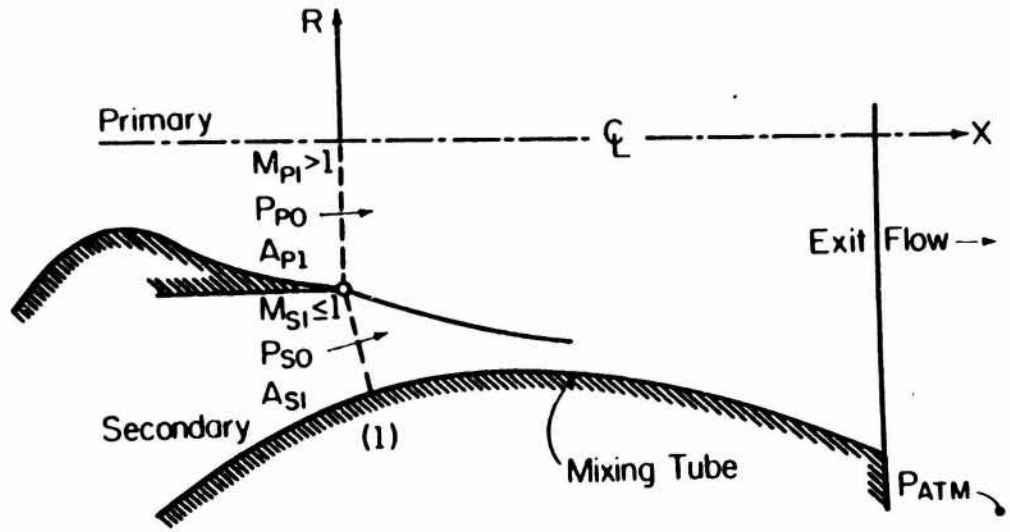


Figure 2.1-1 Ejector configuration and notation

This selection of variables, although less obvious, is convenient for performing the numerical calculations involved in many theoretical ejector analyses.

In addition to establishing the functional form of the pumping characteristics, another quantity of interest is the shroud wall pressure distribution given functionally by:

$$P_w/P_{P0} = f(w_S/w_P, P_{S0}/P_{P0}, P_{ATM}/P_{P0}, x) \qquad (2.1\text{-}3)$$

where x is the axial coordinate.

After establishing the above functional relationships, the thrust characteristics of a system can then be determined in the thrust augmentation application. In practice, this is accomplished by considering the contributions in the axial direction of the entering momentum fluxes of the primary and secondary streams and the integrated shroud wall pressure distribution.

2.1.1.1 Three-dimensional performance surfaces

The functional relations, (2.1-1) and (2.1-2), characterize the "pumping" characteristics of an ejector system and represent surfaces in the spaces described by the coordinates $(w_S/w_P, P_{S0}/P_{P0}, P_{ATM}/P_{P0})$ and $(M_{S1}, P_{S1}/P_{P0}, P_{ATM}/P_{P0})$, respectively.

The pumping characteristics of a typical ejector system in terms of the first set of variables are shown in Fig. 2.1-2. This surface clearly delineates the flow regimes wherein the mass flow characteristics are independent or dependent on the ambient pressure level. These flow regimes merge together along the "break-off curve" and, in principle, this condition serves to uniquely define this curve.

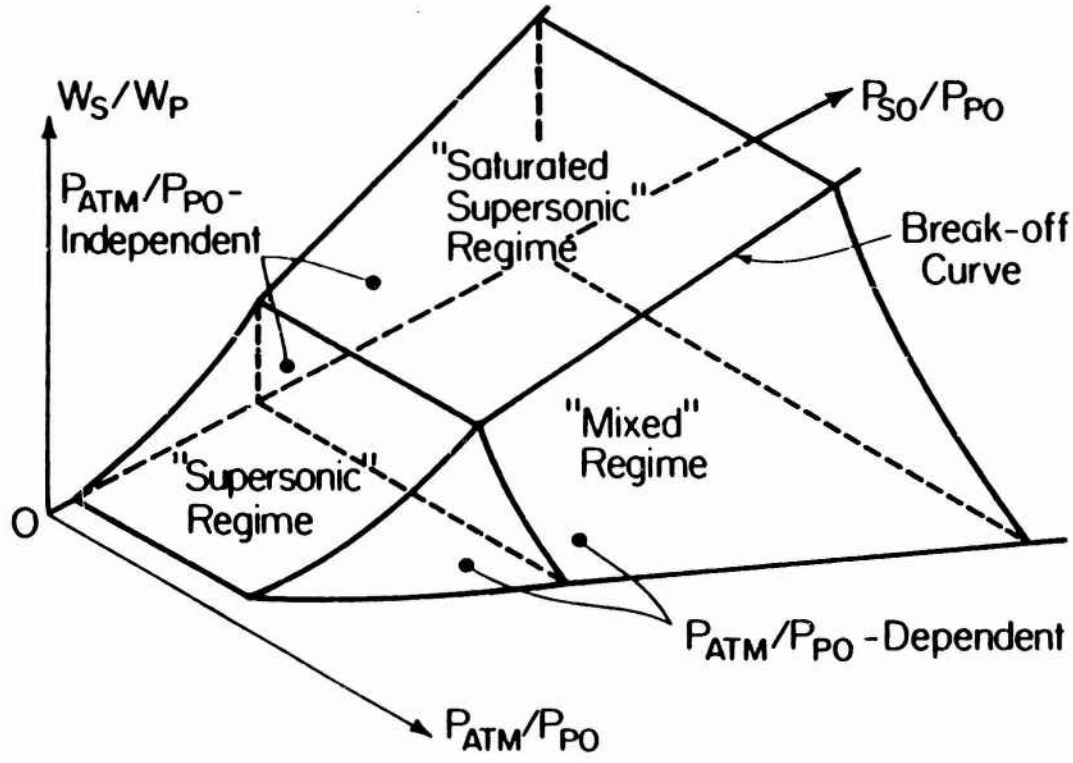


Figure 2.1-2 Ejector mass flow characteristic surface $w_s/w_p = f(P_{so}/P_{po}, P_{ATM}/P_{po})$

To the left of the "break-off curve" ("supersonic" and "saturated supersonic" regimes), the mass flow characteristics are independent of $P_{ATM}/P_{P0}$ and the surface is cylindrical with its generator parallel to the $P_{ATM}/P_{P0}$ axis. For these regimes, the mass flow characteristics can be represented by:

$$w_S/w_P = f(P_{S0}/P_{P0}) \qquad (2.1\text{-}4)$$

when $P_{ATM}/P_{P0} \leq (P_{ATM}/P_{P0})_{BO}$. To the right of the "break-off curve" ("mixed" regime), the surface is three-dimensional in nature and extends from the spatial "break-off curve" to the plane where $w_S/w_P = 0$ (base pressure plane); hence,

$$w_S/w_P = f(P_{S0}/P_{P0}, P_{ATM}/P_{P0}) \qquad (2.1\text{-}5)$$

when $P_{ATM}/P_{P0} \quad (P_{ATM}/P_{P0})_{BO}$.

In principle, the "break-off curve" represents a simultaneous solution of the functional relationships (2.1-4) and (2.1-5). However, the "break-off curve" also has a phenomenological interpretation based on the flowfield interactions occurring within the ejector shroud. Points on the "break-off curve" are determined by the condition that transition from dependence to independence of the mass flow characteristics on the ambient pressure level will occur when the secondary stream just attains sonic conditions either inside the mixing tube or at its entrance. This point will be further amplified in the discussion of the constant-area ejector.

An alternative representation of the pumping characteristics in terms of the variables $(M_{S1}, P_{S1}/P_{P0}, P_{ATM}/P_{P0})$ is given in Fig. 2.1-3.

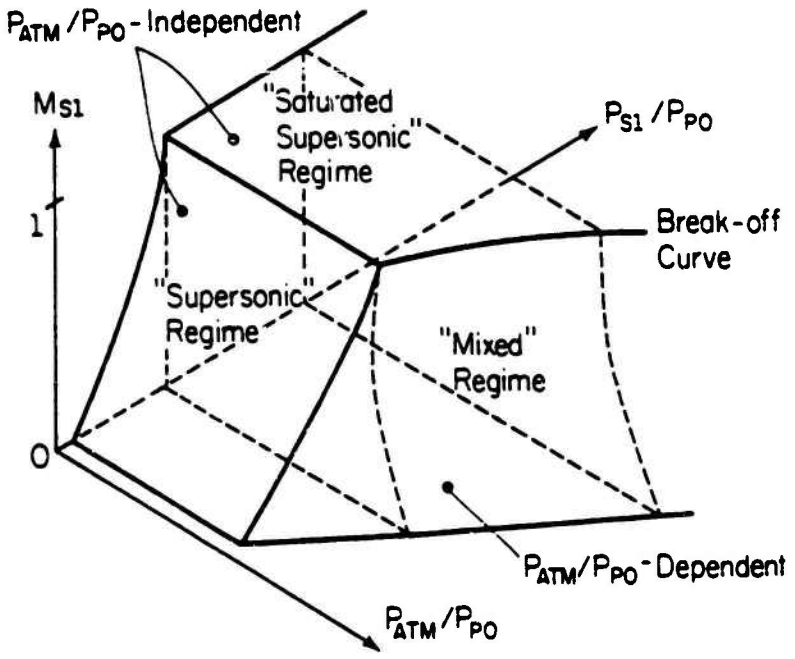


Figure 2.1-3 Ejector characteristic surface $M_{S1} = f(P_{S1}/P_{PO}, P_{ATM}/P_{PO})$

For this surface, there are direct counterparts to the $P_{ATM}/P_{P0}$-independent and $P_{ATM}/P_{P0}$-dependent regimes of the $w_S/w_P$ surface.

2.1.1.2 Two-dimensional parametric curves

The three-dimensional performance surfaces of Figures 2.1-2 and 2.1-3 generally have their principal value in presenting an overview of the performance characteristics of typical ejector systems. In theoretical analyses or experimental programs, it is often more convenient to consider two-dimensional parametric representations of these operating surfaces. These parametric curves usually represent nothing more than intersections of the performance surfaces with various planes corresponding to constant values of the respective variables.

Two of the more useful parametric representations of the mass flow characteristics are obtained by intersecting the $w_S/w_P$ surface by planes of constant $P_{ATM}/P_{P0}$, Fig. 2.1-4, and planes of constant $P_{S0}/P_{P0}$, Fig. 2.1-5. Another interesting and useful parametric curve can be obtained by intersecting the $w_S/w_P$ surface by a plane for which $P_{S0}/P_{P0} = P_{ATM}/P_{P0}$, Fig. 2.1-6. The latter situation corresponds to inducting the secondary fluid at ambient conditions and then discharging the ejector to the same ambient conditions as occurs in thrust augmentation applications.

Also convenient, from the standpoint of theoretical analyses, are intersections of the $M_{S1}$-surface by planes of constant $P_{ATM}/P_{P0}$, Fig. 2.1-7, and planes of constant $P_{S1}/P_{P0}$, Fig. 2.1-8.

It will be of great utility to refer to these three-dimensional solution surfaces and the two-dimensional parametric curves in succeeding discussions of the theoretical models and experimental results.

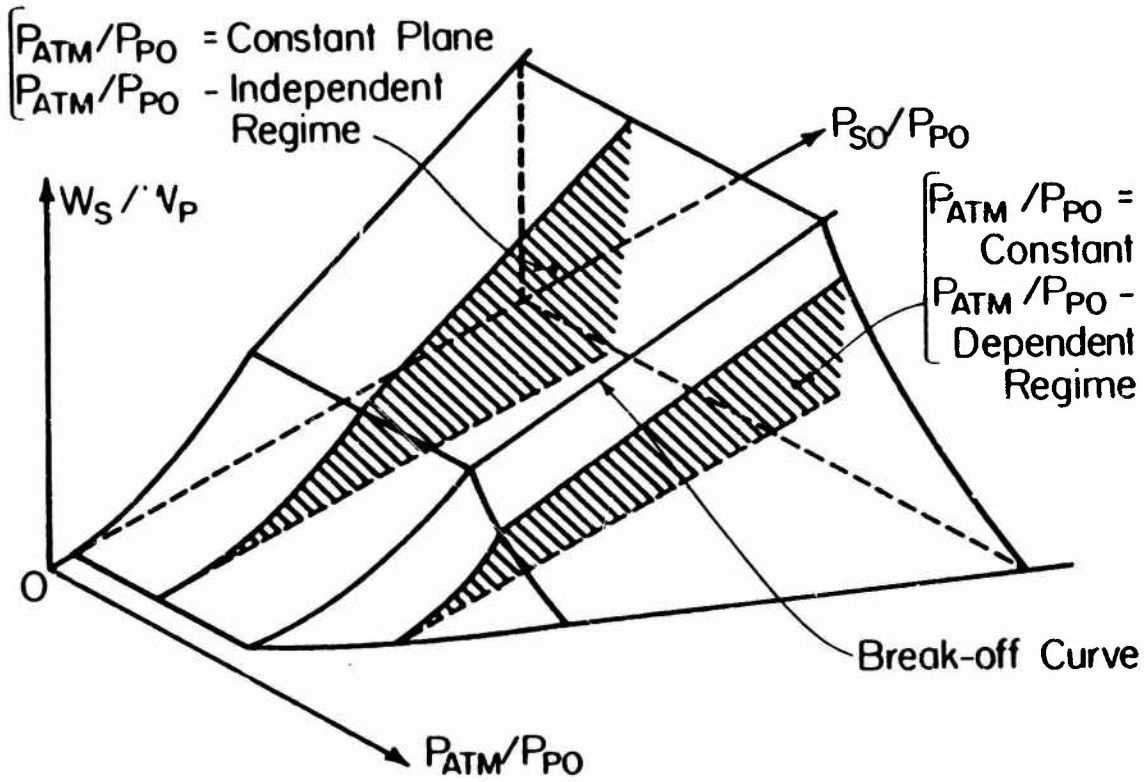


Figure 2.1-4 Intersection of the $w_s/w_p$ surface with planes of constant $P_{ATM}/P_{PO}$

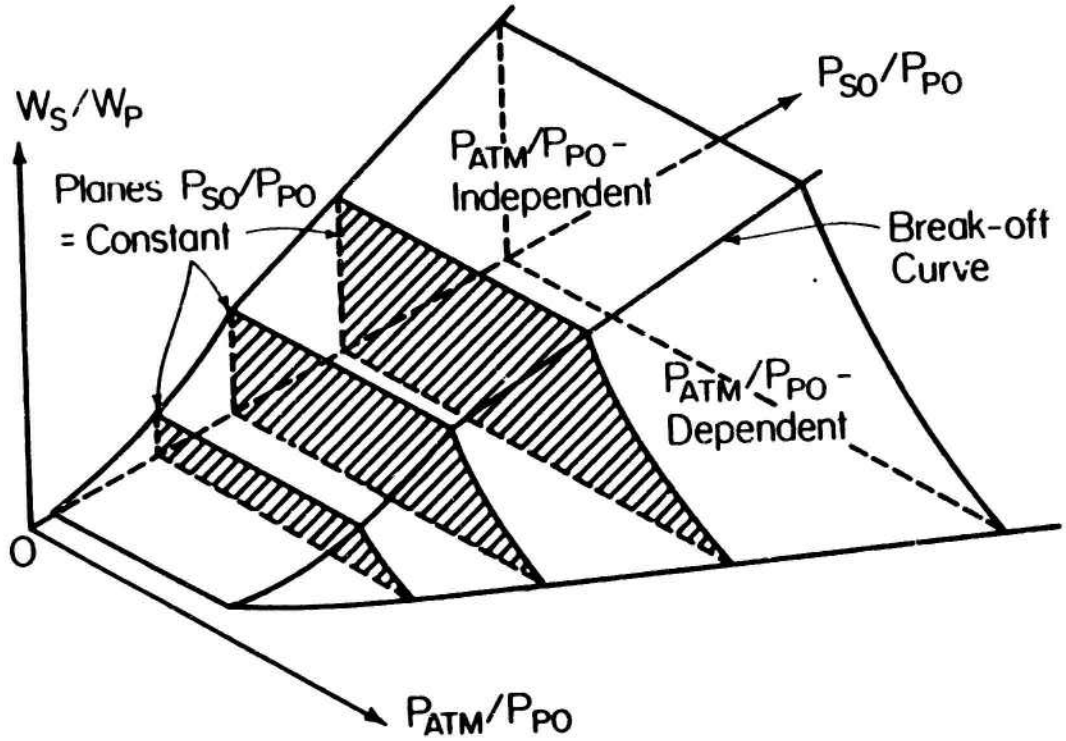


Figure 2.1-5 Intersection of the $w_s/w_p$ surface with planes of constant $P_{so}/P_{po}$

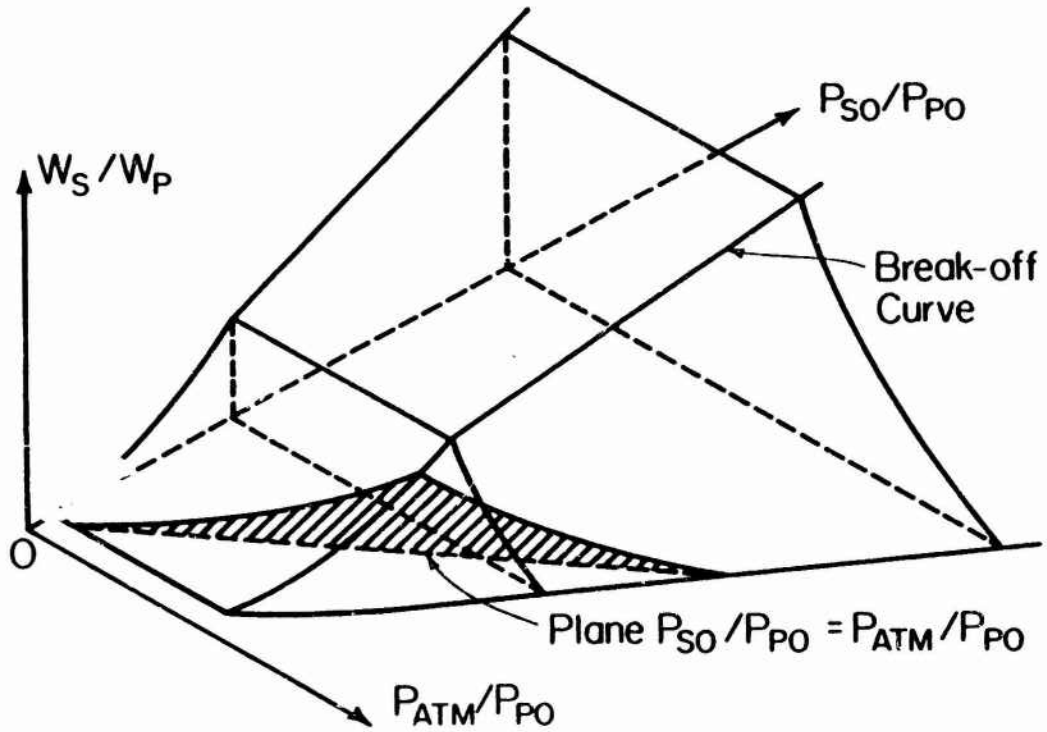


Figure 2.1-6 Intersection of the $w_s/w_p$ surface with a plane $P_{ATM}/P_{PO} = P_{SO}/P_{PO}$

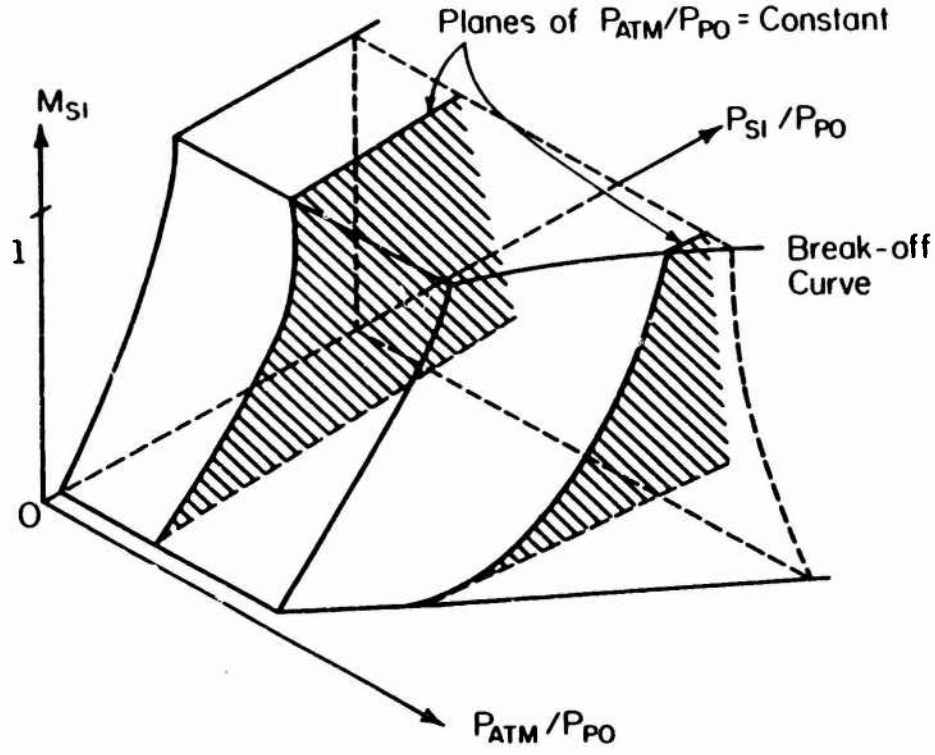


Figure 2.1-7 Intersection of the $M_{S1}$ surface with planes of constant $P_{ATM}/P_{PO}$

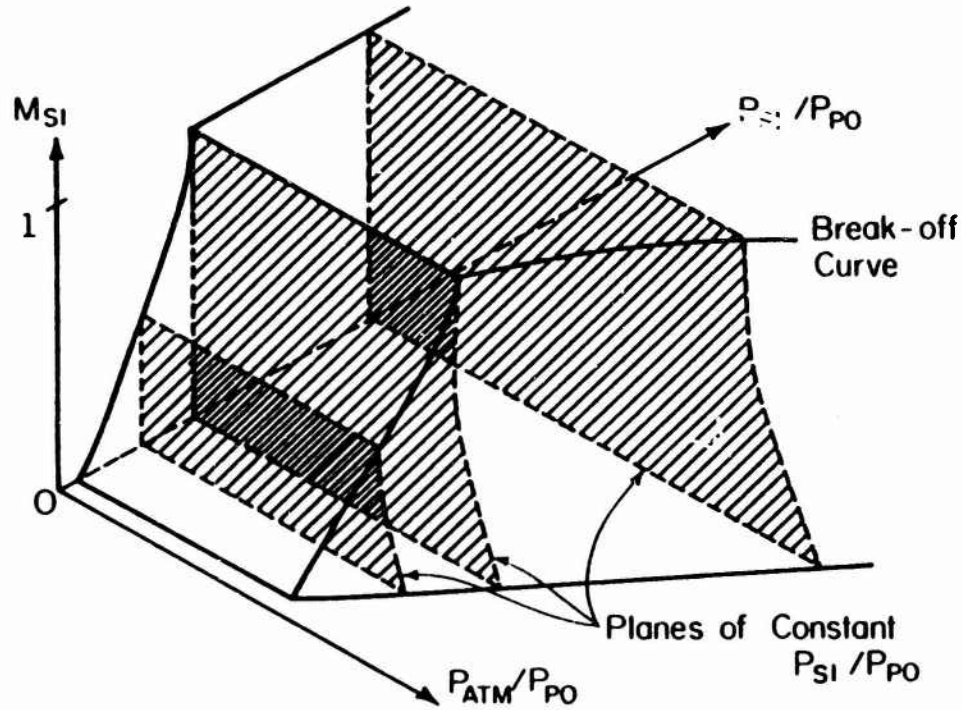


Figure 2.1-8 Intersection of the $M_{S1}$ surface with planes of constant $P_{S1}/P_{PO}$

## 2.2 CONSTANT-PRESSURE EJECTOR

A schematic of a constant-pressure ejector is shown in Fig. 2.2-1. This ejector consists of (1) a variable-area mixing section wherein the primary and secondary flows are assumed to mix to form a uniform supersonic flow and (2) a downstream diffuser section. The analysis of this ejector is based on analyzing separately the operating characteristics of the mixing and diffuser subsystems, and then matching these characteristics to determine the operation of the overall ejector.

The analysis of the flow in the mixing section is based on the principal assumption that the area of the mixing section varies such that the summation of the integrated static pressure-area forces acting on the flow within the mixing section is zero. Of the conceivable geometry-flow combinations that could satisfy the above requirement, the assumption is made that the area of the mixing section varies such that the primary and secondary streams mix at constant static pressure to form a uniform mixed flow. Thus, to satisfy the requirement of constant static pressure in the mixing section, the mixing section area distribution must be different for each operating point of the ejector. While this requirement presents no problems from a theoretical standpoint, it does present several problems from a practical hardware standpoint. The first problem is that the analysis does not provide any information on the mixing section area distribution between the entrance and uniform flow sections, Sections 1 and 2, respectively, in Fig. 2.2-1. The second problem is off-design operation of this ejector. Assuming that an area distribution can be found for which the static pressure is constant for a given ejector geometry and

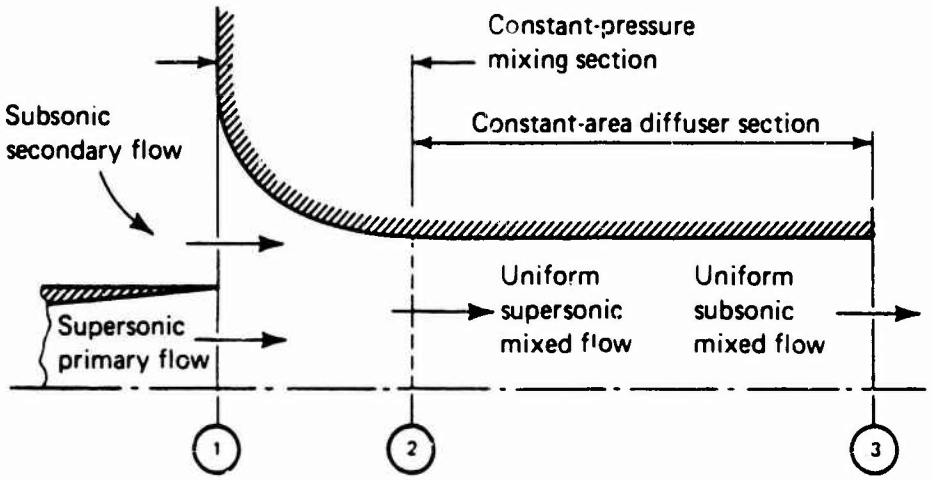


Figure 2.2-1 Constant-pressure ejector configuration

operating point, the operation of this ejector at any point other than the design point would, most probably, result in a significant mismatch of the system and operating conditions, thus causing poor ejector performance.

Downstream of the mixing section, the uniform mixed flow is diffused and discharged to ambient conditions. To analyze the overall ejector performance, a flow model must be adopted for the diffuser section. A simple but adequate approach to this part of the ejector analysis is to assume a constant-area diffuser whose pressure-rise performance can be expressed in terms of the normal-shock pressure rise and an empirical pressure-rise coefficient both of which are determined by the supersonic entrance Mach number to the diffuser.

2.2.1 Constant-pressure ejector analysis

2.2.1.1 Constant-pressure mixing section

The flow in the mixing section is analyzed by applying the conservation equations and numerous assumptions to the control volume shown in Fig. 2.2-2. These assumptions are:

(1) Steady flow, $\frac{\partial(\ )}{\partial t} \equiv 0$.

(2) Piecewise uniform flows at Section 1 and uniform flow at Section 2.

(3) The primary and secondary gases obey the perfect gas relationships.

(4) The primary and secondary streams mix ideally to form a supersonic mixed stream at Section 2.

(5) Negligible shear stresses at the wall.

(6) Adiabatic flow between Sections 1 and 2.

The secondary-to-primary mass flowrate ratio, $\mu \equiv w_s/w_p$, can be expressed in terms of the mass flow function by

$$\mu = \frac{A_{S1}}{A_{P1}} \left[\frac{Mw_S}{Mw_P} \cdot \frac{T_{P0}}{T_{S0}}\right]^{1/2} \frac{f_1(\gamma_S, M_{S1})}{f_1(\gamma_P, M_{P1})} \tag{2.2-5}$$

where assumption (9), $P_{P1} = P_{S1}$, was used. Equation (2.2-3) can also be expressed in terms of the mass flow function by

$$\frac{A_{M2}}{A_{P1}} \left[\frac{Mw_M}{Mw_P} \cdot \frac{T_{P0}}{T_{M0}}\right]^{1/2} \frac{f_1(\gamma_M, M_{M2})}{f_1(\gamma_P, M_{P1})} = (1+\mu) \tag{2.2-6}$$

where $P_{P1} = P_{M2}$ was assumed.

For steady flow, the momentum equation for the flow direction is

$$\leftrightarrow \sum F_x = \oint_{CS} V_x(\rho \bar{V} \cdot d\bar{A}) \quad . \tag{2.2-7}$$

Neglecting wall shear stresses, the summation of forces acting on the control volume in the flow direction is

$$\leftrightarrow \sum F_x = P_{P1}A_{P1} + P_{S1}A_{S1} - P_{M2}A_{M2} - \hat{i}_x \cdot \int_{A_W} P d\bar{A} \tag{2.2-8}$$

or simplifying

$$\leftrightarrow \sum F_x = P_{P1}A_{P1} + P_{S1}A_{S1} - P_{M2}A_{M2} - \int_{A_{M2}}^{A_1} P dA_x \tag{2.2-9}$$

where $A_1 \equiv A_{P1} + A_{S1}$. According to assumption (9), the mixing section area distribution in the flow direction is assumed always to be such that the static pressure along the wall is constant; as a consequence, $\sum F_x = 0$ in Eqs. (2.2-7) to (2.2-9). Hence with assumption (2), Eq. (2.2-7) simplifies to

$$\rho_{P1} V_{P1}^2 A_{P1} + \rho_{S1} V_{S1}^2 A_{S1} = \rho_{M2} V_{M2}^2 A_{M2} \quad . \tag{2.2-10}$$

With assumption (9), $P_{P1} = P_{S1} = P_{M2}$, Eq. (2.2-10) can be expressed in the more convenient form

$$\gamma_P M_{P1}^2 + \frac{A_{S1}}{A_{P1}} \gamma_S M_{S1}^2 = \frac{A_{M2}}{A_{P1}} \gamma_M M_{M2}^2 \quad . \tag{2.2-11}$$

For steady flow, the energy equation is

$$\frac{\partial Q}{\partial t} - \frac{\partial W_{ss}}{\partial t} = \oint_{cs} \left( h + \frac{V^2}{2} + gz \right) \rho \bar{V} \cdot d\bar{A} \quad . \tag{2.2-12}$$

As a consequence of assumptions (6,7,8), the energy equation can be simplified to

$$\oint_{cs} (h_o) \rho \bar{V} \cdot d\bar{A} = 0 \tag{2.2-13}$$

where $h_o \equiv h + \frac{V^2}{2}$ . For the piecewise uniform and uniform flows at Sections (1) and (2), respectively, the energy equation becomes

$$w_P h_{Po} + w_S h_{So} = w_M h_{Mo} \quad . \tag{2.2-14}$$

Using $h_o = C_P T_o$ and $\mu = w_S / w_P$, Eq. (2.2-14) can be combined with Eq. (2.2-3) and the result rewritten as

$$\frac{T_{Mo}}{T_{Po}} = \frac{1}{(1+\mu)} \left[ \frac{(C_P)_P}{(C_P)_M} \right] \left[ 1 + \mu \frac{(C_P)_S}{(C_P)_P} \cdot \frac{T_{So}}{T_{Po}} \right] \quad . \tag{2.2-15}$$

The relationships between the stagnation and static pressures for the primary and secondary flows are determined in the following way. According to assumption (10), the flows between the primary and secondary stagnation states and Section (1) are assumed to be isentropic. Thus, with $P_{S1} = P_{P1}$, the primary to-secondary stagnation pressure ratio is given by

$$\frac{P_{P0}}{P_{S0}} = \frac{f_2(\gamma_S, M_{S1})}{f_2(\gamma_P, M_{P1})} \tag{2.2-16}$$

where the isentropic pressure ratio function $f_2(\gamma,M)$ is defined by

$$\frac{P}{P_0} = \left[1 + \frac{\gamma-1}{2} M^2\right]^{-\gamma/(\gamma-1)} \equiv f_2(\gamma,M) \quad . \tag{2.2-17}$$

The static pressure, $P_{M2}$, at the entrance to the diffuser can be expressed, according to assumption (9), in terms of the secondary stagnation pressure, $P_{S0}$, by

$$\frac{P_{M2}}{P_{S0}} = \frac{P_{S1}}{P_{S0}} = f_2(\gamma_S, M_{S1}) \quad . \tag{2.2-18}$$

The preceding equations are the basis for determining the operating characteristics of the constant-pressure mixing section. However, before these characteristics can be determined, the properties of the mixed gas at Section 2 must be determined and an overall approach to defining and presenting the mixing-tube characteristics must be adopted.

A mixed perfect gas is assumed to exist at Section 2 as a consequence of the mixing of the primary and secondary gases within the mixing section. The properties of the mixed gas are determined by applying Dalton's law of partial pressures to a hypothetical mixing process at constant volume of the respective mass fractions of the primary and secondary perfect gases. From this analysis, the properties of the mixed gas can be expressed by the following relationships in terms of the secondary-to-primary mass flowrate ratio, $\mu$, and the primary and secondary gas properties.

The ratio of specific heats at constant pressure of the primary and mixed gases is

$$\frac{(C_p)_p}{(C_p)_M} = \frac{[1+\mu]}{\left[1 + \mu \frac{(C_p)_s}{(C_p)_p}\right]} \quad . \qquad (2.2\text{-}19)$$

In Eq. (2.2-19), the ratio of specific heats at constant pressure for the secondary and primary gases can be expressed alternatively in terms of other gas properties by

$$\frac{(C_p)_s}{(C_p)_p} = \frac{\gamma_s}{\gamma_p} \cdot \frac{(\gamma_p - 1)}{(\gamma_s - 1)} \cdot \frac{Mw_p}{Mw_s} \quad . \qquad (2.2\text{-}20)$$

The ratio of molecular weights of the primary and mixed gases is given by

$$\frac{Mw_M}{Mw_p} = \frac{(1+\mu)}{\left[1 + \mu \frac{Mw_p}{Mw_s}\right]} \qquad (2.2\text{-}21)$$

The ratio of the specific heat at constant pressure to the specific heat at constant volume for the mixed gas is

$$\gamma_M = \left[1 - \{\frac{\gamma_p - 1}{\gamma_p}\} \frac{\{1 + \mu \frac{Mw_p}{Mw_s}\}}{\{1 + \mu \frac{\gamma_s}{\gamma_p} \cdot \frac{(\gamma_p - 1)}{(\gamma_s - 1)} \cdot \frac{Mw_p}{Mw_s}\}}\right]^{-1} \qquad (2.2\text{-}22)$$

Equations (2.2-19) to (2.2-22) define the mixed gas properties completely in terms of the properties of the primary and secondary gases and the mass flowrate ratio, $\mu$. Thus, any calculational approach is greatly simplified and more straightforward if $\mu$ is assumed to be known, at least parametrically, at the outset. This approach will now be discussed.

There is considerable latitude in determining and presenting the operating characteristics of an ejector. Since the ejector characteristics

are, of course, unique, the preference of one approach or set of variables over another is one of convenience. The basic approach adopted herein is to specify parametrically the secondary-to-primary mass flow-rate ratio, $\mu$, and then to determine the corresponding values of the ejector driving stagnation pressure ratio, $P_{P0}/P_{S0}$, and the overall ejector compression ratio, $P_{M3}/P_{S0}$. Since the operating characteristics of an ejector system can be represented by a three-dimensional surface [1],[†] the foregoing approach simply represents the intersection of this ejector operating surface in $\left(\mu, \frac{P_{P0}}{P_{S0}}, \frac{P_{M3}}{P_{S0}}\right)$ space with planes of $\mu$ = constant.[††]

At the outset, the following data are assumed to be known:

$$\left[\gamma_S, \gamma_P, \frac{Mw_S}{Mw_P}, \frac{T_{S0}}{T_{P0}}, \frac{A_{M2}}{A_{P1}}, M_{P1} > 1\right] .$$

The specification of $A_{M2}/A_{P1}$ instead of $A_{S1}/A_{P1}$ is a convenience for later comparisons between constant-pressure and constant-area ejectors. Utilizing the foregoing data and a parametric value of $\mu$, the mixed gas properties

$$\left[\frac{(C_P)_P}{(C_P)_M}, \frac{Mw_M}{Mw_P}, \gamma_M\right]$$

can be determined from Eqs. (2.2-19), (2.2-21), and (2.2-22), respectively. The mixed-to-primary stagnation temperature ratio, $T_{M0}/T_{P0}$, can then be

---

[†] Numbers in brackets refer to entries in REFERENCES.

[††] Unfortunately, the constant-pressure ejector model is incapable of dealing with this reality of ejector operation. This point will be considered in detail in Section 2.3 wherein the constant-area ejector is analyzed. Note that this selection of variables is somewhat different than those used in Section 2.1.

determined from Eq. (2.2-15). Using these data, the solution value of $M_{M2}$ is determined from Eq. (2.2-6) by solving

$$f_1(\gamma_M, M_{M2}) = \frac{(1+\mu) f_1(\gamma_P, M_{P1})}{\frac{A_{M2}}{A_{P1}}\left[\frac{Mw_M}{Mw_P} \cdot \frac{T_{P0}}{T_{M0}}\right]^{1/2}} \equiv C_1 \quad . \tag{2.2-23}$$

The solution value for $M_{M2}$ (supersonic root) is

$$M_{M2} = \left[\frac{\{\gamma_M^2 + 2\gamma_M(\gamma_M - 1)C_1^2\}^{1/2} - \gamma_M}{\gamma_M(\gamma_M - 1)}\right]^{1/2} \quad . \tag{2.2-24}$$

The next steps in the solution procedure are to determine $A_{S1}/A_{P1}$ and $M_{S1} < 1$. To do this, Eqs. (2.2-5) and (2.2-11) are combined to eliminate tne unknown area ratio, $A_{S1}/A_{P1}$, from the resulting equation. The resulting relationship to be solved for $M_{S1} < 1$ is

$$\frac{f_1(\gamma_S, M_{S1})}{\gamma_S M_{S1}^2} = \frac{\mu f_1(\gamma_P, M_{P1})}{\left[\frac{A_{M2}}{A_{P1}}\gamma_M M_{M2}^2 - \gamma_P M_{P1}^2\right]\left[\frac{Mw_S}{Mw_P} \cdot \frac{T_{P0}}{T_{S0}}\right]^{1/2}} \equiv C_2 \tag{2.2-25}$$

where a finite value with $C_2 > 0$ is required for a meaningful solution. The solution value for $M_{S1}$ is

$$M_{S1} = \left[\frac{2}{1 + (2C_2^2 - 1)\gamma_S}\right]^{1/2} \quad . \tag{2.2-26}$$

After determining $M_{S1} < 1$ from Eq. (2.2-26), the area ratio can then be found by rearranging Eq. (2.2-11)

$$\frac{A_{S1}}{A_{P1}} = \frac{\left[\frac{A_{M2}}{A_{P1}}\gamma_M M_{M2}^2 - \gamma_P M_{P1}^2\right]}{\gamma_S M_{S1}^2} \quad . \tag{2.2-27}$$

The flow through the mixing section is determined by the preceding computational sequence and is characterized by the variables [$M_{S1}$, $A_{S1}/A_{P1}$, $M_{M2}$]. A constant-pressure solution will exist only if

$$\frac{A_{M2}}{A_{P1}} < \left[ \frac{b^2}{\gamma_P M_{P1}^2} - \frac{(\gamma_M - 1)}{2\gamma_M} \gamma_P M_{P1}^2 \right] \tag{2.2-28}$$

where

$$b = (1+\mu) f_1(\gamma_P, M_{P1}) / \left[ \frac{MW_M}{MW_P} \cdot \frac{T_{P0}}{T_{M0}} \right]^{1/2} \tag{2.2-29}$$

If a solution exists, the mixing-section pressure ratios, $P_{P0}/P_{S0}$ and $P_{M2}/P_{S0}$, can then be determined from Eqs. (2.2-16) and (2.2-17), respectively.

To complete the analysis of the constant-pressure ejector, a diffuser must be specified that will diffuse the flow at Section 2 to ambient conditions at the diffuser exit. The simple diffuser model used in this study will be discussed briefly in the next section.

2.2.1.2 Constant-area supersonic diffuser

Supersonic flow entering a constant-area duct is recompressed within the duct by an extended series of shock waves resulting from shock wave-boundary layer interactions. The pressure level to which the flow is recompressed depends on the entering supersonic Mach number and the length-to-diameter ratio of the diffuser duct. Experimental studies have established for various duct cross-sectional area geometries the minimum length-to-diameter ratio of the duct required for the extended shock structure. These data and an empirical correlation based on these data are shown in Fig. 2.2-3; these results are taken from [2].

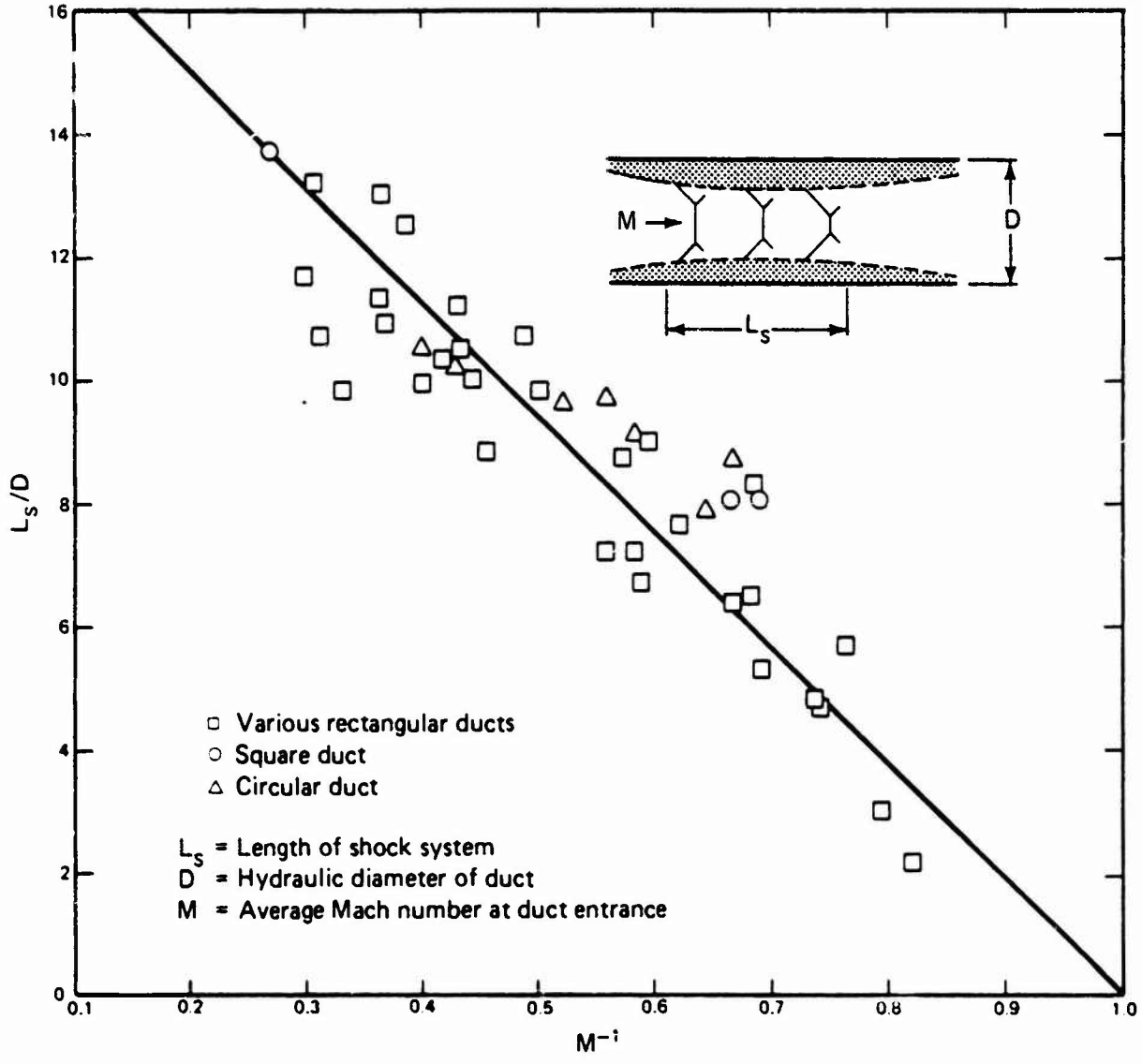


Figure 2.2-3 Empirical correlation for length-to-diameter ratio of constant-area supersonic diffusers (from Reference [2])

Thus, for a duct of sufficient length, the recompression shock system is complete. The pressure rise across this shock system is usually expressed in terms of the pressure rise that would exist across a corresponding normal shock wave of negligible thickness occurring at the duct entrance supersonic Mach number. For the constant-area diffuser of Fig. 2.2-4, the static pressure rise across the duct is expressed by

$$\frac{P_{M3}}{P_{M2}} = r_d f_s(\gamma_M, M_{M2}) \tag{2.2-30}$$

where $r_d$ is an empirical pressure rise coefficient and $f_s(\gamma_M, M_{M2})$ is the normal shock static pressure ratio function. This function is defined by

$$f_s(\gamma, M) = \frac{2\gamma}{(\gamma+1)} M^2 - \frac{(\gamma-1)}{(\gamma+1)} \quad . \tag{2.2-31}$$

The empirical coefficient, $r_d$, accounts for possible incompleteness in the shock recompression system, losses in the diffuser system, etc. For system calculations, the functional behavior of this coefficient must be determined from experiments. Another approach is to vary parametrically the value of $r_d$ to assess the influence of diffuser performance on ejector system operation. As a consequence, the value of $r_d$ is left as an input value to the computer program for estimating constant-pressure ejector performance.†

† Values of $r_d$ in the range, $0.75 < r_d < 1.25$, are commonly used for parametric studies.

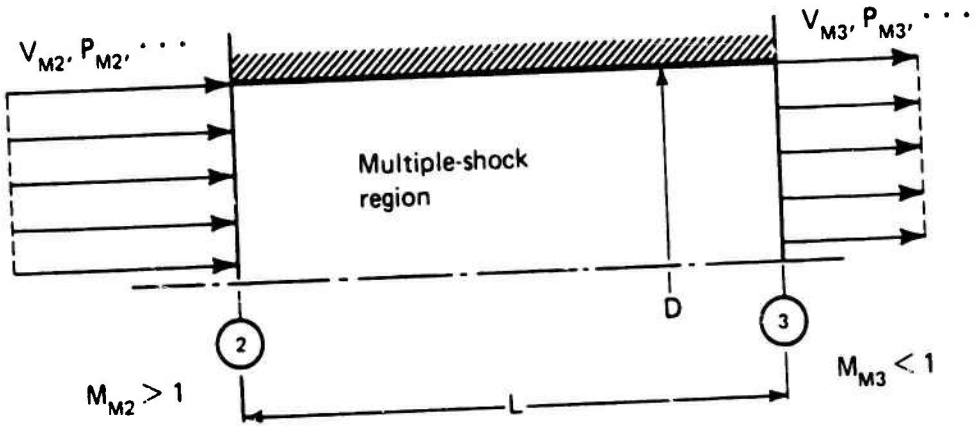


Figure 2.2-4 Constant-area supersonic diffuser notation

2.2.1.3 Overall ejector analysis

The operating characteristics of the constant-pressure mixing section can be determined as outlined in Section 2.2.1.1. For given values of

$$[\gamma_S, \gamma_P, Mw_S/Mw_P, T_{S0}/T_{P0}, A_{M2}/A_{P1}, M_{P1}>1]$$

and a parametric value of $\mu$, the values of

$$[M_{M2}, M_{S1}, A_{S1}/A_{P1}]$$

can be determined. Utilizing these values, the mixing section pressure ratios

$$[P_{P0}/P_{S0}, P_{M2}/P_{S0}]$$

can then be found.

For a given value of the diffuser pressure-rise coefficient, the diffuser static-pressure rise ratio, $P_{M3}/P_{M2}$, can then be determined. The overall ejector compression ratio is determined from

$$\frac{P_{M3}}{P_{S0}} = \frac{P_{M2}}{P_{S0}} \cdot \frac{P_{M3}}{P_{M2}} \qquad (2.2\text{-}32)$$

where $P_{M2}/P_{S0}$ and $P_{M3}/P_{M2}$ are from Eqs. (2.2-18) and (2.2-30), respectively.

The operation of the constant-pressure ejector is then established in terms of the variables $[\mu, P_{P0}/P_{S0}, P_{M3}/P_{S0}]$.

2.2.2 Constant-pressure ejector computer program (CPE)

A computer program was written, based on the analysis of Section 2.2.1, to determine the operating characteristics of constant-pressure ejectors. A complete listing of this program is given in Appendix 6.1.

The input variables, their symbols, and their default values are summarized in Table 2.2-1. The output variables and symbols are summarized in Table 2.2-2.

Table 2.2-1
Input variables for program CPE

| Variable | Symbol | Default value |
|---|---|---|
| $\gamma_S$ | GS | 1.405 |
| $\gamma_P$ | GP | 1.405 |
| $Mw_S/Mw_P$ | MWSP | 1.0 |
| $T_{S0}/T_{P0}$ | TSØPØ | 1.0 |
| $A_{M2}/A_{P1}$ | AM2P1 | --- |
| $M_{P1}$ | MP1 | --- (>1.0) |
| $r_d$ | RD | 1.0 |
| $\mu=w_S/w_P$ | WSPI | --- |
| --- | CASE | "NEW" |

Table 2.2-2
Output variables for program CPE

| Variable | Symbol |
|---|---|
| $\gamma_M$ | GM |
| $Mw_M/Mw_P$ | MWMP |
| --- | NCASE |
| $M_{M2}$ | MM2 |
| $M_{S1}$ | MS1 |
| $A_{S1}/A_{P1}$ | AS1P1 |
| $P_{P0}/P_{S0}$ | PPØSØ |
| $P_{M3}/P_{S0}$ | PM3SØ |

2.2.3 Representative results

To demonstrate typical operating characteristics of a constant-pressure ejector, the ejector configuration summarized in Table 2.2-3 was selected.

Table 2.2-3
Representative constant-pressure ejector configuration

| Variable | Value |
|---|---|
| $\gamma_S$ | 1.4 |
| $\gamma_P$ | 1.4 |
| $Mw_S/Mw_P$ | 1.0 |
| $T_{S0}/T_{P0}$ | 1.0 |
| $A_{M2}/A_{P1}$ | 3.0, 4.0 |
| $M_{P1}$ | 4.0 |
| $r_d$ | 1.0 |
| $\mu$ | Varied |

The operating characteristics of this ejector system are summarized in Fig. 2.2-5. From this figure, it is clear that the constant-pressure ejector solution exists for each area ratio over only a relatively small range of mass flowrate ratios. Corresponding to this range, the value of $M_{S1}$ varies throughout its possible range, $0 < M_{S1} \leq 1$. The compression ratio for this ejector is highest for relatively small values of $M_{S1}$; this is the reason that $M_{S1} = 0.20$ is often chosen in discussions of the theoretical performance of this type of ejector. In the neighborhood of small values of $M_{S1}$, it is seen that $A_{S1}/A_{P1}$ varies significantly.

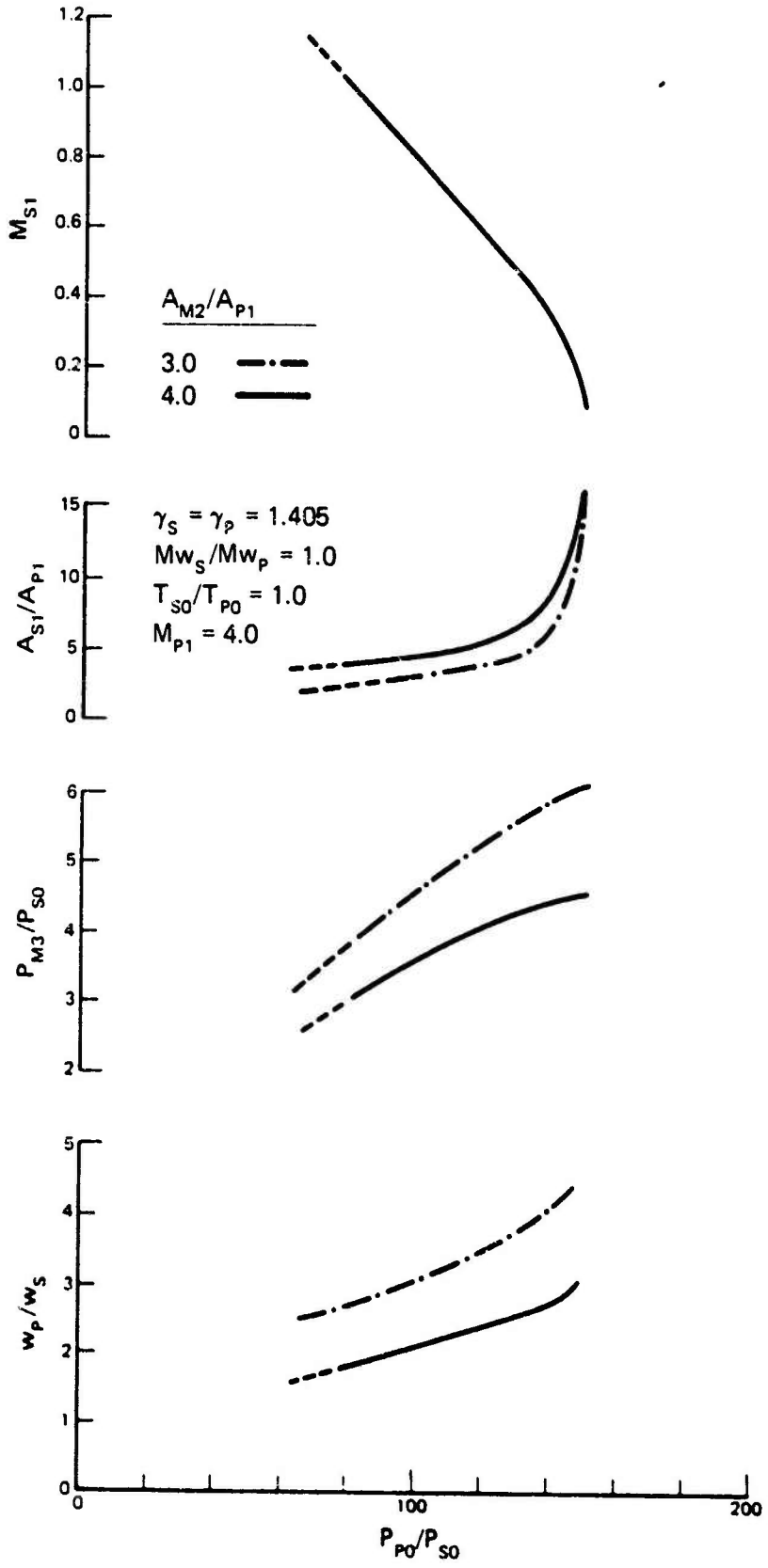


Figure 2.2-5 Representative characteristics for a constant-pressure ejector

This constant-pressure ejector configuration was chosen for comparison with a constant-area ejector with a similar configuration, Section 2.3.3.

A comparison of the compression pressure ratio characteristics of the constant-pressure ejector (Fig. 2.2-5) and constant-area ejectors (Figs. 2.3-4b,d) with the same values of $A_{M2}/A_{P1}$ and $M_{P1}$, shows that both ejectors have approximately the same maximum compression pressure ratios. However, the constant-area ejector is seen to have a much broader range of possible solutions.

Due to the large number or variables involved, no attempt was made to present herein a comprehensive parametric study of the constant-pressure ejector or expected trends as a consequence of variations in these variables. Rather, it is recommended that the computer program be used to make these studies only after a baseline configuration has been established.

## 2.3 CONSTANT-AREA EJECTOR

A schematic of a constant-area ejector is shown in Fig. 2.3-1. The ejector consists of a constant-area mixing section wherein the primary and secondary flows interact and mix to form a uniform mixed flow at the ejector exit. The constant-area ejector has two distinct operating regimes which are identified according to whether the mass flowrate characteristics of the ejector are dependent or independent of the back-pressure level imposed at the ejector exit. In the literature [3,4], the back-pressure dependent regime is referred to as the "mixed" regime and the back-pressure independent regime as the "supersonic" and

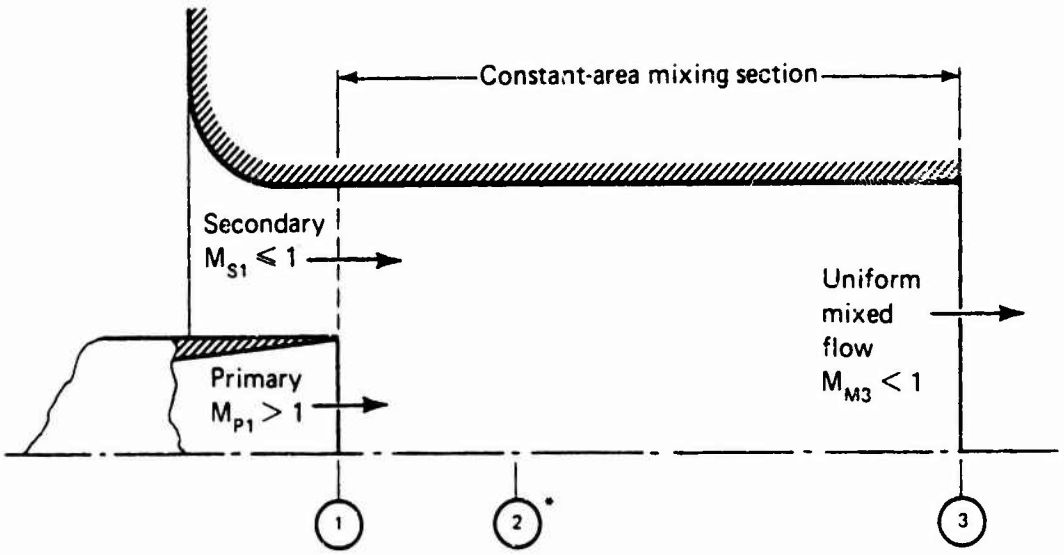


* Exists only for the "supersonic" regime

Figure 2.3-1 Constant-area ejector configuration

"saturated-supersonic" regimes. While these designations are somewhat misnomers, they do, however, describe the operating regimes of an ejector in analogy to a conventional converging-diverging nozzle [1].

The performance of an ejector system can only be analyzed by establishing both the conditions for these flow regimes to exist and the conditions for transition between these regimes. The transition conditions between the "mixed" and "supersonic" or "saturated-supersonic" regimes are referred to as the "break-off" conditions.

The "supersonic" regime of an ejector is the result of the nearly inviscid interaction between the primary and secondary streams downstream of their confluence, Section 1, Fig. 2.3-1. The static pressures at the confluence of the flows must be such that the supersonic primary flow expands and interacts with the subsonic secondary flow causing it to reach sonic flow conditions at the aerodynamically formed minimum secondary flow area. As a consequence of this secondary flow choking phenomenon, the secondary mass flowrate is determined independent of back-pressure conditions. While the ejector mass flowrate characteristics are independent of the back-pressure level, the complex shock, mixing, and interaction flow structure that governs the pressure recovery is dependent on the back-pressure level.

The "saturated-supersonic" regime is a limiting case of the "supersonic" regime. The ejector conditions are such that the secondary flow reaches sonic flow conditions at the geometric minimum area at the confluence of the primary and secondary flows (Section 1). Again, the mass flowrate characteristics of the ejector are independent of the back-pressure conditions while the recompression flow process is not.

The "mixed" regime includes all ejector operating conditions for which the secondary mass flowrate is dependent on the back-pressure level. This dependency is the result of the secondary flow not attaining sonic flow conditions at either the confluence of the streams or within the downstream interaction region. Consequently, both the secondary mass flowrate and the ejector recompression process are dependent on the back-pressure level.

The criteria for determining the "break-off" conditions are derived from the requirement that a continuous transition between the "supersonic" or "saturated-supersonic" regimes and the "mixed" regime must exist. These criteria and the determination of the "break-off" conditions are important factors in analyzing and understanding ejector operation.

The constant-area ejector has been analyzed by a detailed interaction model [1,5] which has been generalized to include variable-area mixing section ejectors [6]. While the operational characteristics predicted with this model are in good agreement with experiment, the computational time requirements and complexities eliminate this technique as an effective method for making broad-band parametric studies of ejector operation. As a consequence, the study herein is restricted to the constant-area ejector which exhibits all of the operational characteristics of more complex geometries but yet can still be analyzed by simplified one-dimensional methods. The one-dimensional analysis provides results that are generally in good agreement with experiment except at small secondary flowrates when $P_{s1} < P_{p1}$. The reason for this breakdown in the flow model is well-known [1,5]; essentially, the reason is that the flowfield shifts from being one-dimensional in nature to a flowfield that is two-dimensional in nature. This change in flowfield character is the direct

result of the expanding supersonic primary flow interacting with the mixing-section wall. Thus, the one-dimensional analysis would be expected to yield poor results for this flow regime. This deficiency in the flow model should not cause significant problems as long as there is an awareness of the existence and causes of the problem.

The components of the constant-area ejector model, their analyses, and the computational approach will now be discussed.

2.3.1 Constant-area ejector analysis

The ejector flow model consists of essentially two components. One component is the overall analysis of the constant-area mixing section, Sections 1 to 3. The other component is the analysis of the nearly inviscid interaction region just downstream of the confluence of the primary and secondary flows. These components are incorporated into an analysis from which the "break-off" conditions, the mass flowrate characteristics, and the compression characteristics can be determined.

This analysis is based on the work of Fabri, et al., [3,4].

2.3.1.1 <u>One-dimensional overall mixing-section analysis</u>

The control volume used in the overall mixing section analysis is shown in Fig. 2.3-2. The piecewise uniform primary and secondary flows at Section 1 are assumed to interact and to mix within the mixing section to form a uniform mixed flow at Section 3. As a consequence of the existence of the "mixed" and "supersonic" or "saturated-supersonic" regimes, the application of the conservation relations to this control volume does not, in general, result in a unique solution for the flow in the mixing section. As a consequence, additional conditions must be imposed to find a unique solution for the "supersonic" and

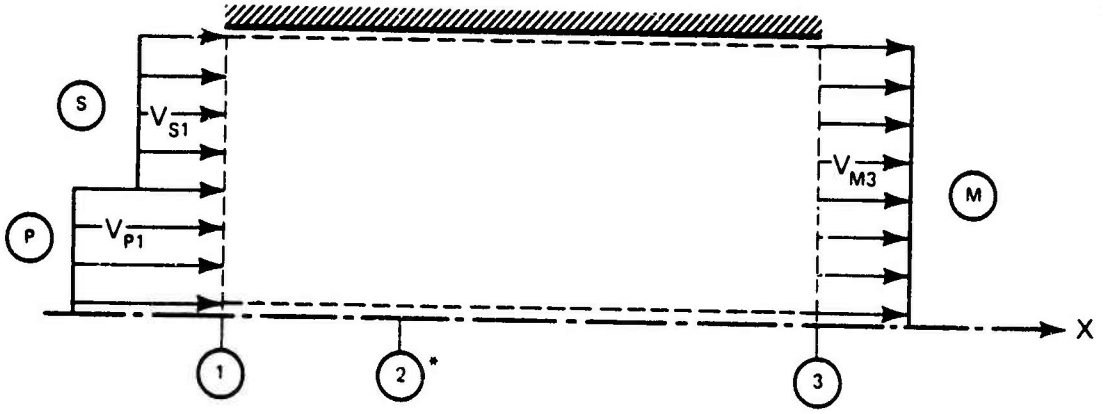


---- Control volume

P, $\rho$, A, V, T, M, etc. are defined for each stream at sections 1 and 3.

* If "choking" exists

Figure 2.3-2 Constant-area mixing section control volume

"saturated-supersonic" regimes since the secondary mass flowrate characteristics are independent of the back-pressure level at Section 3 for these regimes. The additional conditions required for a unique solution are provided by the secondary flow choking phenomenon which is the result of the interaction of the primary and secondary flows downstream of their confluence. No additional conditions are required for the "mixed" regime other than satisfying the boundary condition at the ejector exit plane that the exit-plane pressure is equal to the ambient pressure level. The transition between these regimes defines the "break-off" conditions, i.e., the conditions for which a unique solution can be found that simultaneously satisfies the "supersonic" or "saturated-supersonic" regimes and the "mixed" regime.

The analysis of the overall mixing section is based on the application of the conservation equations and the following assumptions to the control volume of Fig. 2.3-2. The assumptions are:

(1) Steady flow, $\frac{\partial(\ )}{\partial t} \equiv 0$.

(2) Piecewise uniform flows at Section 1 and uniform flow at Section 3.

(3) The primary and secondary gases obey the perfect gas relationships.

(4) The primary and secondary streams mix ideally to form a mixed stream at Section 3.

(5) Negligible shear stresses at the wall.

(6) Adiabatic flow between Sections 1 and 3.

(7) No shaft or shear work between Sections 1 and 3.

(8) A negligible change in potential energy due to variations in elevation in the mixing section.

(9) The primary and secondary flows are assumed to be isentropic from their respective stagnation states to the states at Section 1.

The continuity equation is

$$\oint_{CS} \rho \bar{V} \cdot d\bar{A} = 0 \qquad (2.3\text{-}1)$$

and with assumption (2) becomes

$$\rho_{P1} V_{P1} A_{P1} + \rho_{S1} V_{S1} A_{S1} = \rho_{MS} V_{MS} A_{MS} \quad . \qquad (2.3\text{-}2)$$

In terms of the mass flowrates, $w = \rho AV$, the continuity equation is

$$w_S + w_P = w_M \quad . \qquad (2.3\text{-}3)$$

The mass flowrate, w, is expressed in terms of the mass flow function by

$$\frac{w}{PA}\left[\frac{R}{Mw} \cdot T_0\right]^{1/2} = M\left[\gamma\{1 + \frac{(\gamma-1)}{2} M^2\}\right]^{1/2} \equiv f_1(\gamma, M) \quad . \qquad (2.3\text{-}4)$$

Introducing the secondary-to-primary mass flowrate ratio, $\mu \equiv w_S/w_P$, and Eq. (2.3-4) into Eq. (2.3-3) results in an expression for the static pressure ratio $P_{MS}/P_{P1}$. The result is

$$\frac{P_{MS}}{P_{P1}} = \left[\frac{Mw_P}{Mw_M} \cdot \frac{T_{MO}}{T_{PO}}\right]^{1/2} \left[\frac{A_{P1}}{A_{MS}}\right] \frac{f_1(\gamma_P, M_{P1})}{f_1(\gamma_M, M_{MS})} (1+\mu) \qquad (2.3\text{-}5)$$

In terms of the mass flow function, the mass flowrate ratio, $\mu$, is

$$\mu = \frac{P_{S1}}{P_{P1}} \cdot \frac{A_{S1}}{A_{F1}} \left[\frac{Mw_S}{Mw_P} \cdot \frac{T_{PO}}{T_{SO}}\right]^{1/2} \frac{f_1(\gamma_S, M_{S1})}{f_1(\gamma_P, M_{P1})} \quad . \qquad (2.3\text{-}6)$$

The static pressure ratio, $P_{S1}/P_{P1}$, can be expressed from Eq. (2.3-6) as

$$\frac{P_{S1}}{P_{P1}} = \frac{A_{P1}}{A_{S1}} \left[\frac{Mw_P}{Mw_S} \cdot \frac{T_{S0}}{T_{P0}}\right]^{1/2} \frac{f_1(\gamma_P, M_{P1})}{f_1(\gamma_S, M_{S1})} \mu \quad . \tag{2.3-7}$$

The momentum equation in the flow direction is

$$\leftrightarrow \sum F_x = \oint_{CS} V_x(\rho \bar{V} \cdot d\bar{A}) \quad . \tag{2.3-8}$$

With the foregoing assumptions, the momentum equation becomes

$$P_{P1}A_{P1} + P_{S1}A_{S1} - P_{M3}A_{M3} = \rho_{M3}A_{M3}V_{M3}^2 - (\rho_P A_{P1}V_{P1}^2 + \rho_{S1}A_{S1}V_{S1}^2) \quad . \tag{2.3-9}$$

Equation (2.3-9) can be expressed in a more convenient form by

$$\frac{P_{S1}}{P_{P1}} \cdot \frac{A_{S1}}{A_{P1}} \left(1+\gamma_S M_{S1}^2\right) + \left(1+\gamma_P M_{P1}^2\right) = \frac{P_{M3}}{P_{P1}} \cdot \frac{A_{M3}}{A_{P1}} \left(1+\gamma_M M_{M3}^2\right) \tag{2.3-10}$$

Equations (2.3-5). (2.3-7), and (2.3-10) can be combined and rearranged into a form that is particularly convenient for computation; the result is

$$f_3(\gamma_M, M_{M3}) = \frac{f_3(\gamma_P, M_{P1}) + f_3(\gamma_S, M_{S1}) \left[\frac{Mw_P}{Mw_S} \cdot \frac{T_{S0}}{T_{P0}}\right]^{1/2} \mu}{\left[\frac{Mw_P}{Mw_M} \cdot \frac{T_{M0}}{T_{P0}}\right]^{1/2} (1+\mu)} \tag{2.3-11}$$

where the function $f_3(\gamma, M)$ is defined as

$$f_3(\gamma, M) = \frac{(1+\gamma M^2)}{M\left[\gamma\{1 + \frac{\gamma-1}{2} M^2\}\right]^{1/2}} \tag{2.3-12}$$

The relationship, $f_3(\gamma, M)$ = constant, can be solved for the Mach number, M, as

$$M = \left\{ \frac{-\left[f_3^2-2\right] \pm \left[\left[f_3^2-2\right]^2 + 2\left[\frac{\gamma-1}{\gamma}\right]\left[f_3^2 - \frac{2\gamma}{(\gamma-1)}\right]\right]^{1/2}}{(\gamma-1)\left[f_3^2 - \frac{2\gamma}{(\gamma-1)}\right]} \right\}^{1/2} \tag{2.3-13}$$

The energy equation is

$$\frac{\partial Q}{\partial t} - \frac{DW_{ss}}{Dt} = \oint_{cs} \left(h + \frac{V^2}{2} + gZ\right)(\rho \bar{V} \cdot d\bar{A}) \quad . \tag{2.3-14}$$

With simplifying assumptions (6,7,8), the energy equation becomes

$$\oint_{cs} h_0 (\rho \bar{V} \cdot d\bar{A}) = 0 \tag{2.3-15}$$

where $h_0 = h + V^2/2$. For the overall mixing section control volume, the energy equation becomes

$$w_P h_{P0} + w_S h_{S0} = w_M h_{M0} \quad . \tag{2.3-16}$$

The continuity and energy equations can be combined along with $h_0 = C_P T_0$ and $\mu = w_S/w_P$ to develop an expression for the mixed-to-primary stagnation temperature ratio. The result is

$$\frac{T_{M0}}{T_{P0}} = \frac{1}{(1+\mu)} \left[\frac{(C_P)_P}{(C_P)_M}\right]\left[1 + \mu \frac{(C_P)_S}{(C_P)_P} \cdot \frac{T_{S0}}{T_{P0}}\right] \quad . \tag{2.3-17}$$

The secondary-to-primary stagnation pressure ratio can be expressed by

$$\frac{P_{S0}}{P_{P0}} = \frac{P_{S1}}{P_{P1}} \cdot \frac{(P_{P1}/P_{P0})}{(P_{S1}/P_{S0})} \tag{2.3-18}$$

where the pressure ratios $P_{P1}/P_{P0}$ and $P_{S1}/P_{S0}$ are by assumption (9) determined for isentropic flow. For isentropic flow, the pressure ratio function is defined by

$$\frac{P}{P_0}(\gamma, M) = \left[1 + \frac{\gamma-1}{2} M^2\right]^{-\gamma/(\gamma-1)} \equiv f_2(\gamma, M) \quad . \tag{2.3-19}$$

Thus, Eq. (2.3-18) becomes

$$\frac{P_{S0}}{P_{P0}} = \frac{P_{S1}}{P_{P1}} \cdot \frac{f_2(\gamma_P, M_{P1})}{f_2(\gamma_S, M_{S1})} \quad . \tag{2.3-20}$$

In the preceding equations, the gas properties of the mixed flow at Section 3 must be known. These properties are determined for the mixed gas by applying Dalton's law of partial pressures to a hypothetical mixing process at constant volume for the respective mass fractions of the primary and secondary perfect gases. The mixed gas properties are expressed in terms of the secondary-to-primary mass flowrate ratio and the primary and secondary gas properties by

$$\frac{(C_p)_P}{(C_p)_M} = \frac{(1+\mu)}{\left[1 + \mu \dfrac{(C_p)_S}{(C_p)_P}\right]} \quad , \tag{2.3-21}$$

$$\frac{Mw_M}{Mw_P} = \frac{(1+\mu)}{\left[1 + \mu \dfrac{Mw_P}{Mw_S}\right]} \quad , \tag{2.3-22}$$

and

$$\gamma_M = \left\{1 - \left\{\frac{\gamma_P - 1}{\gamma_P}\right\} \frac{\left\{1 + \mu \dfrac{Mw_P}{Mw_S}\right\}}{\left\{1 + \mu \dfrac{\gamma_S}{\gamma_P} \dfrac{(\gamma_P - 1)}{(\gamma_S - 1)} \dfrac{Mw_P}{Mw_S}\right\}}\right\}^{-1} \quad . \tag{2.3-23}$$

The ratio of specific heats at constant pressure can be expressed in terms of other properties by

$$\frac{(C_p)_S}{(C_p)_P} = \frac{\gamma_S}{\gamma_P} \cdot \frac{(\gamma_P - 1)}{(\gamma_S - 1)} \cdot \frac{Mw_P}{Mw_S} \quad . \tag{2.3-24}$$

Equations (2.3-21) to (2.3-24) define the mixed gas properties completely in terms of the properties of the primary and secondary gases and the mass flowrate ratio, $\mu$.

The computational procedure adopted herein will now be discussed.

At the outset, the following data are assumed to be known

$$\left[\gamma_S,\ \gamma_P,\ \frac{Mw_S}{Mw_P},\ \frac{T_{S0}}{T_{P0}},\ \frac{A_{MS}}{A_{P1}},\ M_{P1} > 1\right] \quad .$$

If the primary nozzle base area is assumed to be negligible, the constant-area mixing section requirement is

$$\frac{A_{S1}}{A_{P1}} = \left[\frac{A_{MS}}{A_{P1}} - 1\right] \quad . \tag{2.3-25}$$

Using these data and a parametric value of $\mu$, the mixed gas properties at Section 3 can be determined from Eqs. (2.3-21) to (2.3-23); the results are

$$\left[\frac{(C_p)_P}{(C_p)_M},\ \frac{Mw_M}{Mw_P},\ \gamma_M\right] \quad .$$

The mixed-to-primary flow stagnation temperature ratio, $T_{M0}/T_{P0}$, can then be found from Eq. (2.3-17)

An examination of Eqs. (2.3-5), (2.3-7), and (2.3-11) shows that the following variables are still to be determined; they are

$$\left[M_{S1} \leq 1,\ \frac{P_{S1}}{P_{P1}},\ M_{MS},\ \frac{P_{MS}}{P_{P1}}\right] \quad .$$

Thus, this set of equations must be supplemented, as discussed in the foregoing sections, with an additional relationship before unique ejector solutions can be determined. The needed relationship is between the

variables $M_{S1}$ and $P_{S1}/P_{P1}$ for a parametric value of $\mu$. The form of this relationship, as will be discussed in the following sections, is determined by the operating regime.

Thus, with the aforementioned input data, a parametric value of $\mu$, and a presumed relationship between ($M_{S1}$, $P_{S1}/P_{P1}$), all values at Section 3 can be determined by the foregoing analysis.

The subroutine, CAEOCV(...), has been written, based on the foregoing analysis for the overall control volume, to carry out the computations as just described. The subroutine has the form

```
CAEOCV (GP, MP1, GS, MS1, MWSP, TSØPØ, PS1P1, AP1M3, NERROR,
                MM3, PPØSØ, PM3SØ, PMØSØ).
```

For input values of (GP, MP1, GS, MS1, MWSP, TSØPØ, PS1P1, AP1M3), the subroutine either returns a set of solution values for (MM3, PM3SØ, PM3S1, PPØSØ, PMØSØ) or a no-solution error indicator NERROR.

A listing of this subroutine is included in Appendix 6.2.

2.3.1.2 Ejector flow regimes and their criteria

The relationship between the static pressures, $P_{S1}$ and $P_{P1}$, determines the operating regime of an ejector.

If $P_{S1} \geq P_{P1}$, the ejector operates in either the "saturated-supersonic" or the "mixed" regime because (1) the minimum secondary flow area is equal to the geometric secondary flow area at Section 1, and (2) the secondary flow is subsonic upstream of Section 1 thus limiting $M_{S1}$ to the range, $0 < M_{S1} \leq 1$. For the "saturated-supersonic" regime, the secondary flow is sonic at Section 1, $M_{S1} = 1$, and the secondary mass flowrate is determined solely by the upstream conditions. For the "mixed"

regime, the secondary flow at Section 1 is subsonic, $M_{s1} < 1$, and the secondary mass flowrate is dependent on both the upstream and downstream conditions.

If $P_{s1} < P_{p1}$, the ejector operates in either the "supersonic" or the "mixed" regime. In both regimes, the primary flow expands and interacts with the secondary flow to form a minimum secondary flow area, i.e., an "aerodynamic" throat, in the primary-secondary interaction region, Section 2, Figs. 2.3-2, 2.3-3. Since the secondary flow is subsonic upstream of this minimum-area location, specifically $M_{s1} < 1$, the secondary flow Mach number at the minimum-area location is limited to $M_{s2} \leq 1$. For the "supersonic" regime, the secondary flow is sonic at the minimum-area location, $M_{s2} = 1$, and the secondary mass flowrate is determined solely by the conditions at and upstream of the minimum-area location. For the "mixed" regime, the secondary flow is subsonic at the minimum-area location, $M_{s2} < 1$, and the secondary mass flowrate is dependent on both the conditions upstream and downstream of the minimum-area location.

The determination of the break-off conditions for transition from one operating regime to another is an important consideration in the analysis of an ejector system. The possible transitions are between:

(1) The "saturated-supersonic" and "supersonic" regimes,

(2) The "saturated-supersonic" and "mixed" regimes, and

(3) The "supersonic" and "mixed" regimes.

The criteria for determining each transition are based on the relationship between the pressures, $P_{s1}$ and $P_{p1}$, and the Mach number at the minimum flow area, either Section 1 or 2 as the case may be. If the Mach number

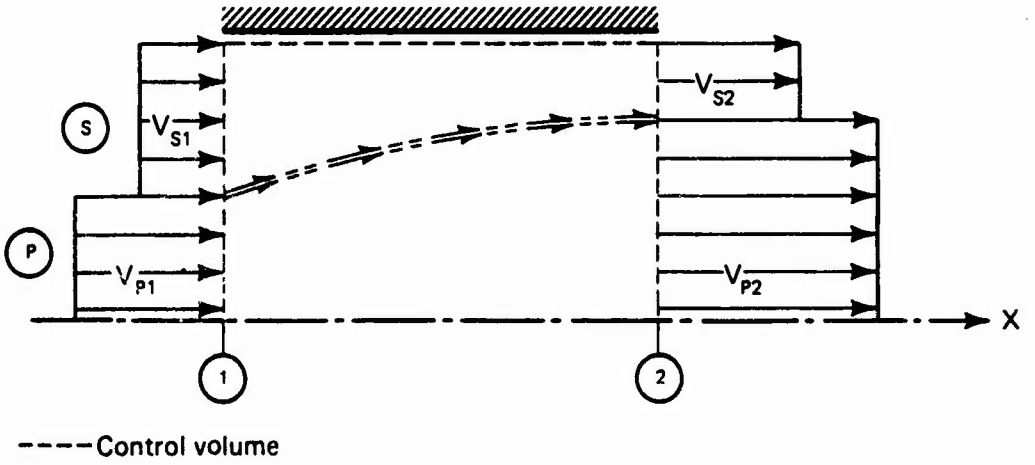


Figure 2.3-3 Control volume for Fabri "choking" analysis

at the minimum flow area is unity, the ejector operates in either the "saturated-supersonic" or the "supersonic" regime; while if this Mach number is less than unity, the ejector operates in the "mixed" regime.

The break-off conditions for transition between the various regimes must satisfy the following conditions. They are:

(1) For the juncture of the "saturated-supersonic" and "supersonic" regimes: $(M_{S1})_{BO} = 1$ and $(P_{S1}/P_{P1})_{BO} = 1$;

(2) For the "saturated-supersonic" and "mixed" regimes: $(M_{S1})_{BO} = 1$ and $(P_{S1}/P_{P1})_{BO} \geq 1$; and

(3) For the "supersonic" and "mixed" regimes: $(M_{S1})_{BO} < 1$, $(P_{S1}/P_{P1})_{BO} \leq 1$, and $(M_{S2})_{BO} = 1$.

For case (3), the transition requirements are special since the value of $(M_{S1})_{BO} < 1$ must be determined based on the requirements that $(P_{S1}/P_{P1})_{BO} < 1$ and $(M_{S2})_{BO} = 1$. The flow model and analysis due to Fabri, et al. [3,4], for analyzing the "supersonic" regime will now be discussed.

The control volume for this analysis extends between Sections 1 and 2, Fig. 2.3-3. In addition to the assumptions listed in Section 2.3.1.1, the following additional assumptions are made:

(1) The streams remain distinct and do not mix between Sections 1 and 2.

(2) The flow is isentropic for each stream between Sections 1 and 2.

(3) The average pressures of the streams can be different at each cross-section.

(4) The Mach number of the secondary flow at Section 2 is

$M_{S2} = 1$.

(5) The static pressures at the mixing tube inlet are such that $P_{P1} > P_{S1}$.

For an assumed value of $M_{S1}$, and since $M_{S2} = 1$, the secondary flow area at Section 2 can be expressed in terms of the secondary flow area at Section 1 by the isentropic area-ratio function

$$\frac{A_{S1}}{A_{S2}} = \frac{A}{A^*}(\gamma_S, M_{S1}) = f_4(\gamma_S, M_{S1}) \tag{2.3-26}$$

where

$$\frac{A}{A^*}(\gamma, M) = M^{-1}\left[\frac{2}{(\gamma+1)} \cdot \{1 + \frac{\gamma-1}{2} M^2\}\right]^{(\gamma+1)/2(\gamma-1)} \tag{2.3-27}$$

The primary flow Mach number $M_{P2}$ is determined from the available flow area at Section 2 and the assumption of isentropic flow between Sections 1 and 2. Since $A_{MS} = (A_{S1}+A_{P1}) = (A_{S2}+A_{P2})$ = constant, the isentropic area-ratio function to be solved for $M_{P2}$ is

$$\frac{A}{A^*}(\gamma_P, M_{P2}) = f_4(\gamma_P, M_{P2}) = \frac{\left[1 - \frac{(1-A_{P1}/A_{MS})}{(A_{S1}/A_{S2})}\right]}{(A_{P1}/A_{MS})} \cdot \frac{A}{A^*}(\gamma_P, M_{P1}) \tag{2.3-28}$$

where $f_4(\gamma_P, M_{P2}) \geq 1$ is necessary and the supersonic branch of the A/A* function is used.

The momentum equation for this flow and the control volume shown in Fig. 2.3-3 is

$$P_{S1}A_{S1}(1+\gamma_S M_{S1}^2) + P_{P1}A_{P1}(1+\gamma_P M_{P1}^2) = P_{S2}A_{S2}(1+\gamma_S) + P_{P2}A_{P2}(1+\gamma_P M_{P2}^2) \quad . \tag{2.3-29}$$

This expression can be rearranged into a more convenient form to determine $P_{S1}/P_{P1}$; the relationship is

$$\frac{P_{S1}}{P_{P1}} = \frac{\left[\frac{(P_{P2}/P_{P0})}{(P_{P1}/P_{P0})} \cdot \frac{(A_{P2}/A_P^*)}{(A_{P1}/A_P^*)} \left(1+\gamma_P M_{P2}^2\right) - \left(1+\gamma_P M_{P1}^2\right)\right]}{\left[\frac{1-(A_{P1}/A_{MS})}{A_{P1}/A_{MS}}\right]\left[(1+\gamma_S M_{S1}^2) - \frac{(P_{S2}/P_{S0})}{(P_{S1}/P_{S0})} \cdot \frac{(1+\gamma_S)}{(A_{S1}/A_S^*)}\right]} \qquad (2.3\text{-}30)$$

In Eq. (2.3-30), the functions ($P_{P2}/P_{P0}$, $P_{P1}/P_{P0}$, $P_{S2}/P_{S0}$, $P_{S1}/P_{S0}$) and ($A_{P1}/A_P^*$, $A_{P2}/A_P^*$, $A_{S1}/A_S^*$) are determined from the isentropic pressure-ratio and area-ratio functions, Eqs. (2.3-19) and (2.3-27), respectively.

Thus, for the "supersonic" regime, a value of $P_{S1}/P_{P1}$ can be determined for an assumed value of $M_{S1}$ and given values of ($\gamma_S$, $\gamma_P$, $M_{P1}$, $A_{P1}/A_{MS}$). This then provides the necessary additional relationship between the variables to determine the "supersonic" ejector operating characteristics and the transition between the "supersonic" and "mixed" regimes.

A computer subroutine, CAEFC(...), has been written based on the foregoing analysis of the Fabri criterion for "choking" in a constant-area ejector. This subroutine has the form

CAEFC(GP, MP1, GS, MS1, AP1M3, PS1P1, NERROR, NTYPE)

where for input values of (GP, MP1>1, GS, MS1<1, AP1M3) the subroutine will return a value of PS1P1 and a value of the iteration control variable NTYPE or an error indicator NERROR.

A listing of this subroutine is included in Appendix 6.2.

Assume for the moment that the break-off values are known for each of the three transition cases; then with the analysis of Section 2.3.1.1, the break-off values at Section 3, i.e., {$(M_{MS})_{BO}$, $(P_{MS}/P_{P1})_{BO}$, etc.)} can

be determined for each case. Thus, ranges of these variables can be determined for operation within the various ejector operating regimes.

For the actual operation of an ejector, the operating regime is determined by the relationship between the externally imposed pressure boundary condition, $P_{ATM}$, at Section 3 and the break-off values. The usual operation of an ejector is with $M_{M3} < 1$ and thus $P_{M3} = P_{ATM}$ required. Consequently, the ejector operating regime is determined by the relationship between $P_{ATM}$ and the break-off values $(P_{M3})_{BO}$.

2.3.1.3 Computational procedure

As is the case in many compressible flow problems, it is more convenient to establish the overall operating characteristics of the ejector rather than to determine the operating characteristics for a specific set of conditions. This is the approach taken herein.

The operational characteristics of the constant-area ejector are investigated and presented in terms of the variables ($\mu$, $P_{P0}/P_{S0}$, $P_{L3}/P_{S0}$)†. For given values of ($\gamma_S$, $\gamma_P$, $Mw_S/Mw_P$, $A_{P1}/A_{M3}$, $T_{S0}/T_{P0}$, $M_{P1} > 1$), the mass flowrate ratio, $\mu$ = constant, is specified parametrically and the range and solution values of ($P_{P0}/P_{S0}$, $P_{M3}/P_{S0}$) are to be determined.

The first step in this procedure is to determine, for the parametric value of $\mu$, whether the ejector would operate in the "saturated-supersonic" or "supersonic" regime for a very low back pressure. This determination is made in the following way. At the juncture between the "saturated-supersonic" and "supersonic" regimes, $(M_{S1})_{BO} = 1$ and

---

†Note that this choice of variables is somewhat different than those used in Section 2.1.

$(P_{S1}/P_{P1})_{BO} = 1$. For these conditions, the value of $\mu$ at the juncture of these regimes, $\mu_j$, is calculated from Eq. (2.3-6). If $\mu > \mu_j$, then the ejector would operate in the "saturated-supersonic" regime and the break-off would be between the "saturated-supersonic" and "mixed" regimes. However, if $\mu < \mu_j$, then the ejector would operate in the "supersonic" regime and the break-off would be between the "supersonic" and "mixed" regimes.

For the "saturated-supersonic" regime, $\{(M_{S1})_{BO} = 1, (P_{S1}/P_{P1}) \geq 1\}$, the corresponding break-off values of $(P_{MB}/P_{S0})_{BO}$ and $(P_{P0}/P_{S0})_{BO}$ are determined from the analysis presented in Section 2.3.1.1. The remainder of the ejector operating characteristics in the "mixed" regime are determined by arbitrarily varying $M_{S1}$ in the range $(M_{S1})_{Min} < M_{S1} < 1$ and then determining the flow conditions at Section 3 for this flow to exist. For an assumed value of $M_{S1}$ in this range, the value of $P_{S1}/P_{P1}$ is determined for the parametric value of $\mu$ from Eq. (2.3-7); the lower limit for $M_{S1}$ in this analysis is set by arbitrarily limiting $P_{S1}/P_{P1}$ to the range

$$(P_{S1}/P_{P1})_{BO} < P_{S1}/P_{P1} < (P_{S1}/P_{P1})_{MAX}$$

where $(P_{S1}/P_{P1})_{MAX}$ is the static-pressure ratio at which a normal shock wave would stand at the nozzle exit plane, i.e.,

$$\left(\frac{P_{S1}}{P_{P1}}\right)_{MAX} = \frac{P_Y}{P_X}(\gamma_P, M_{P1}) = f_5(\gamma_P, M_{P1}) \quad . \tag{2.3-31}$$

The values of the variables $(P_{MB}/P_{S0}, P_{P0}/P_{S0})$ for this flow to exist are then determined according to the analysis of Section 2.3.1.1 for the "mixed" regime.

For the "supersonic" regime and the parametric value of $0 < \mu < \mu_j$, the values of $\{(M_{S1})_{BO} < 1, (P_{S1}/P_{P1})_{BO} < 1\}$ must be determined by an iterative procedure. The procedure followed is to assume a value of $(M_{S1})_i$ in the range $0 < (M_{S1})_i < 1$; from Section 2.3.1.2, a value of $(P_{S1}/P_{P1})_i$ can be determined. With these values of $\{(M_{S1})_i, (P_{S1}/P_{P1})_i\}$ $\mu_i$ can be determined from Eq. (2.3-6). The iteration proceeds until a value of $(M_{S1})_i$ is found that satisfies the convergence requirement

$$\varepsilon > \left|1 - \frac{\mu_i}{\mu}\right| > 0$$

where $\varepsilon$ is nominally taken as $10^{-4}$. This procedure establishes the break-off values of $\{(M_{S1})_{BO}, (P_{S1}/P_{P1})_{BO}\}$ for the "supersonic" regime. The remainder of the break-off values $\{(P_{MS}/P_{SO})_{BO}, (P_{PO}/P_{SO})_{BO}\}$ for the "supersonic" regime are determined according to the analysis of Section 2.3.1.1

The remainder of the ejector operating characteristics in the "mixed" regime are determined by arbitrarily varying $M_{S1}$ in the range $(M_{S1})_{MIN} < M_{S1} < (M_{S1})_{BO}$. For the assumed value of $M_{S1}$ in this range, the value of $P_{S1}/P_{P1} > (P_{S1}/P_{P1})_{BO}$ is determined for the parametric value of $\mu$ from Eq. (2.3-7); again, the lower limit for $M_{S1}$ in this analysis is set by arbitrarily limiting $P_{S1}/P_{P1}$ to the range

$$(P_{S1}/P_{P1})_{BO} < P_{S1}/P_{P1} < \frac{P_Y}{P_X}(\gamma_P, M_{P1}) \quad .$$

For each set of values $(\mu, M_{S1}, P_{S1}/P_{P1})$, the values of the variables $(P_{MS}/P_{SO}, P_{PO}/P_{SO})$ for this flow to exist are then determined according to the analysis of Section 2.3.1.1 for the "mixed" regime.

These analyses have been incorporated into a computer program for convenience of calculation. This program will now be briefly discussed.

2.3.2 Constant-area ejector computer program (CAE)

The constant-area ejector program, CAE(...), is based on the analyses presented in the preceding sections. The program is written in FORTRAN IV and is listed in Appendix 6.2.

The program is organized from the following constant-area ejector (CAE...) and miscellaneous subroutines. They are:

(1) CAE: Main program.

(2) CAENZF(...): Non-zero flow ejector characteristics.

(3) CAEOCV(...): Overall control volume analysis for the mixing section.

(4) CAEFC(...): Fabri criterion for "choked" flow.

(5) MSAR(...): $M^* = f(\gamma, A/A^*)$ for isentropic flow.

(6) ITER(...): Iteration control subroutine.

The input variables and their computer symbols, default values, and input format are given in Table 2.3-1.

The output from CAE can be selected in either of two forms depending on the value of PRINT. For the default value, PRINT = 'ALL', the ejector break-off conditions, operating regime for low back pressure, and operating and compression characteristics are determined for the input values of the system variables and the parametric value of $\mu$, WSPI. Then the operating characteristics are determined within the "mixed" regime at a number of discrete points, or until the maximum value of $P_{S1}/P_{P1}$ is reached. Thus, a cut is made through the ejector operating

| Table 2.3-1<br>Input for program CAE | | |
|---|---|---|
| Variable | Symbol | Default value |
| $\gamma_S$ | GS | 1.405 |
| $\gamma_P$ | GP | 1.405 |
| $Mw_S/Mw_P$ | MWSP | 1.0 |
| $A_{P1}/A_{M3}$ | AP1M3 | ---† |
| $M_{P1}$ | MP1 | ---† |
| $T_{S0}/T_{P0}$ | TSØPØ | 1.0 |
| $\mu = w_S/w_P$ | WSPI | ---† |
| --- | CASE | "NEW" |
| --- | PRINT | "ALL" |

†These data values must be input for at least the first case in a series of cases.

Notes: (1) The input format is by NAMELIST: $ICAE ... $END.

(2) See main program comments for CAE, Section 6.2.1.

surface at a value of $\mu$ = constant. In this way, the overall ejector operating characteristics can be established. These data ($\mu$, $P_{P0}/P_{S0}$, $P_{M3}/P_{S0}$), are suitable for three-dimensional graphical presentations or as a step in an iteration procedure to determine a specific ejector operating point for a specified set of conditions.

For the input value, PRINT = 'BO', only the ejector break-off conditions, operating regime for low back pressure, and operating and compression characteristics are determined for the input values of the system variables and the parametric value of $\mu$, WSPI.

The output variables and their computer symbols are summarized in Table 2.3-2.

Table 2.3-2
Output for program CAE

| Variable | Symbol |
|---|---|
| $M_{S1}$ | MS1 |
| $P_{S1}/P_{P1}$ | PS1P1 |
| $M_{MS}$ | MM3 |
| --- | NCASE |
| $P_{P0}/P_{S0}$ | PPØPSØ |
| $P_{MS}/P_{S0}$ | PM3SØ |
| $P_{M0}/P_{S0}$ | PMØSØ |

Notes: (1) The regimes are identified by: "saturated-supersonic" regime ≡ SSR; "supersonic" regime ≡ SR; and "mixed" regime ≡ MR.

(2) The input variables and current values are printed for each case.

2.3.3 Representative results

To demonstrate typical operating characteristics of a constant-area ejector, the ejector configuration summarized in Table 2.3-3 was selected.

The mass flowrate ratio characteristics for the back-pressure independent regime are shown in Fig. 2.3-4(a) for $M_{P1}$ = 4.0 and

$A_{P1}/A_{M3}$ = 0.25, 0.333 and Fig. 2.3-4(e) for $M_{P1}$ = 5 and $A_{P1}/A_{M3}$ = 0.25. The compression pressure ratio characteristics are given in Figs. 2.3-4 (b,c,d).

Table 2.3-3
Representative constant-area ejector configuration

| Variable | Value |
|---|---|
| $\gamma_S$ | 1.405 |
| $\gamma_P$ | 1.405 |
| $MW_S/MW_P$ | 0.5, 1.0, 2.0 |
| $T_{S0}/T_{P0}$ | 1.0 |
| $A_{P1}/A_{b3}$ | 0.25, 0.333 |
| $M_{P1}$ | 4.0, 5.0 |
| $w_P/w_S$ | 2.0-20.0 |

The compression pressure ratio characteristics are a convenient aid in understanding the operational characteristics of an ejector system. Referring to Fig. 2.3-4(b), the lower-left to upper-right band of curves represents the "mixed" regime and forms the break-off curve as the locus of "break-off" points. For any given $w_p/w_s$, the "mixed" regime follows one of these curves up to the "break-off" point where the compression curve becomes a vertical line for either the "SR" or "SSR" corresponding to the value of $w_p/w_s$. The back-pressure independent regimes are on or below the "break-off" curve. The "MR," "SSR," and "SR" are also shown in the figure.

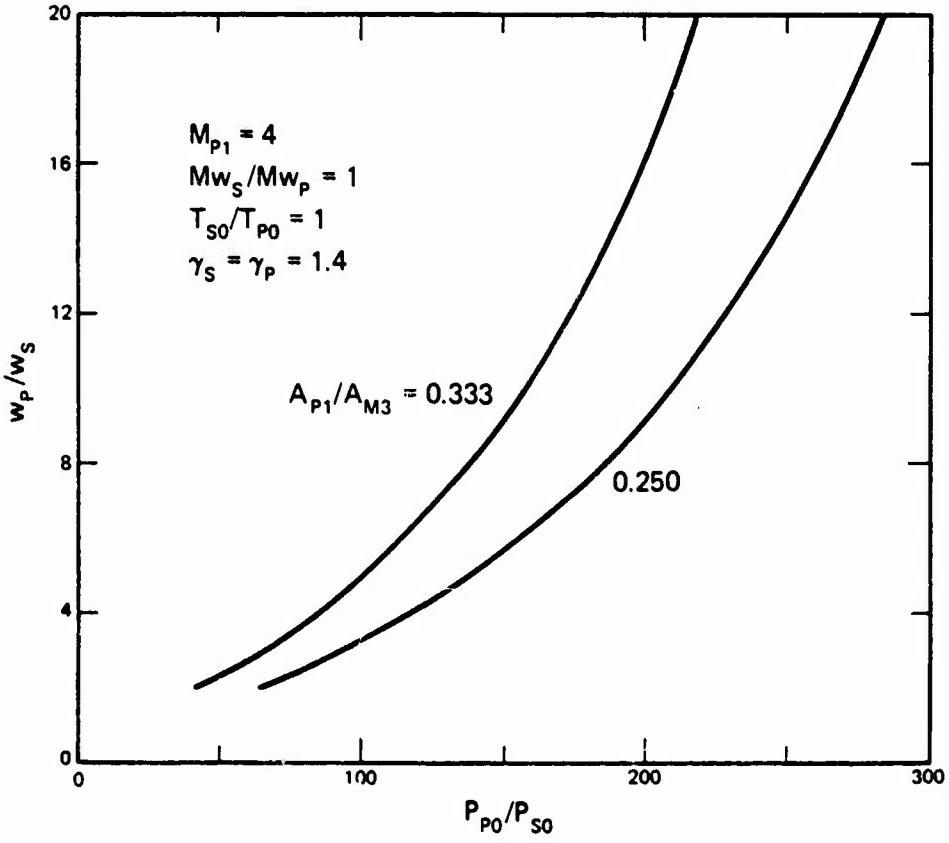


(a) Mass flowrate characteristics

Figure 2.3-4 Constant-area ejector characteristics

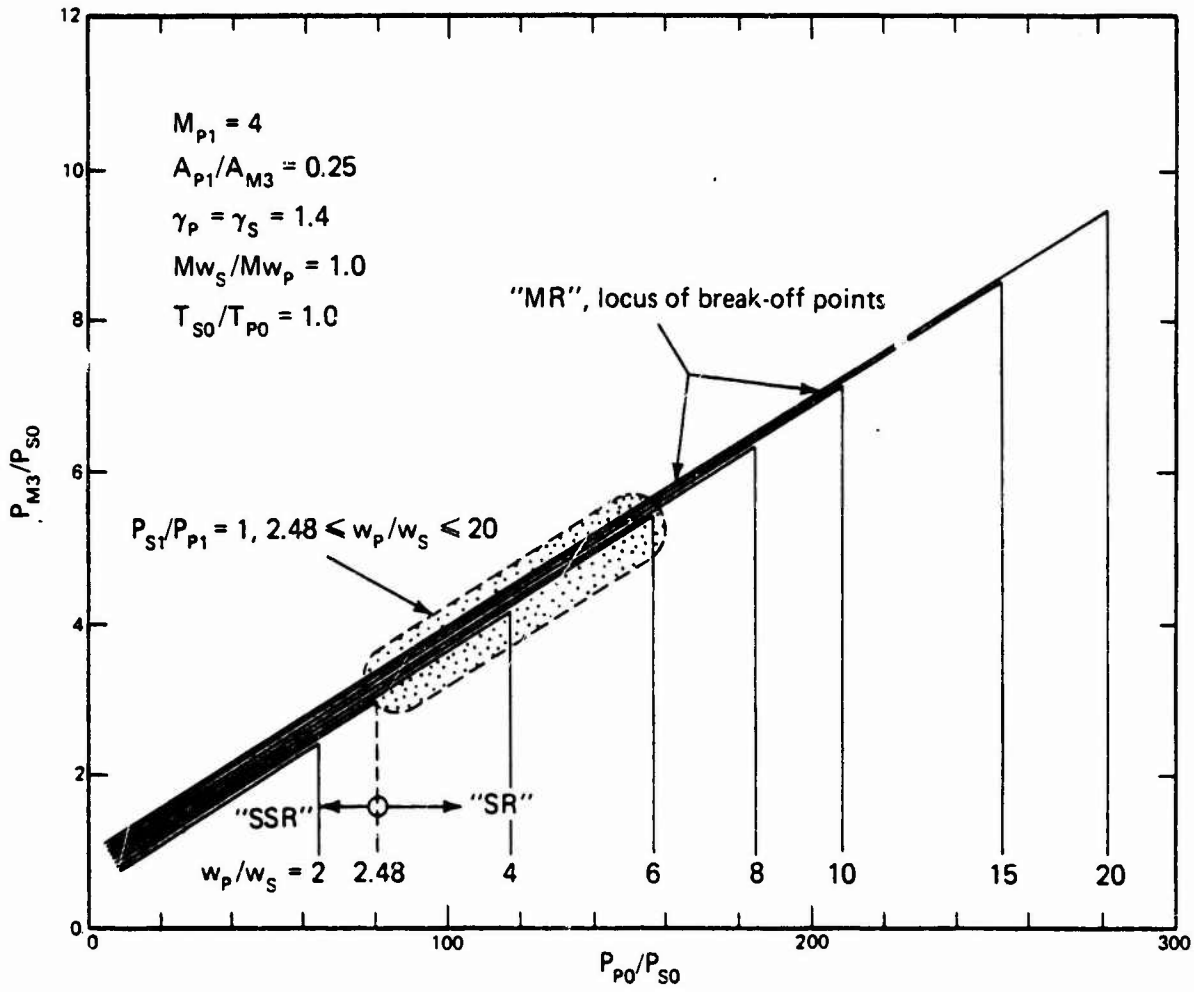


(b) Compression characteristics

Figure 2.3-4 Continued

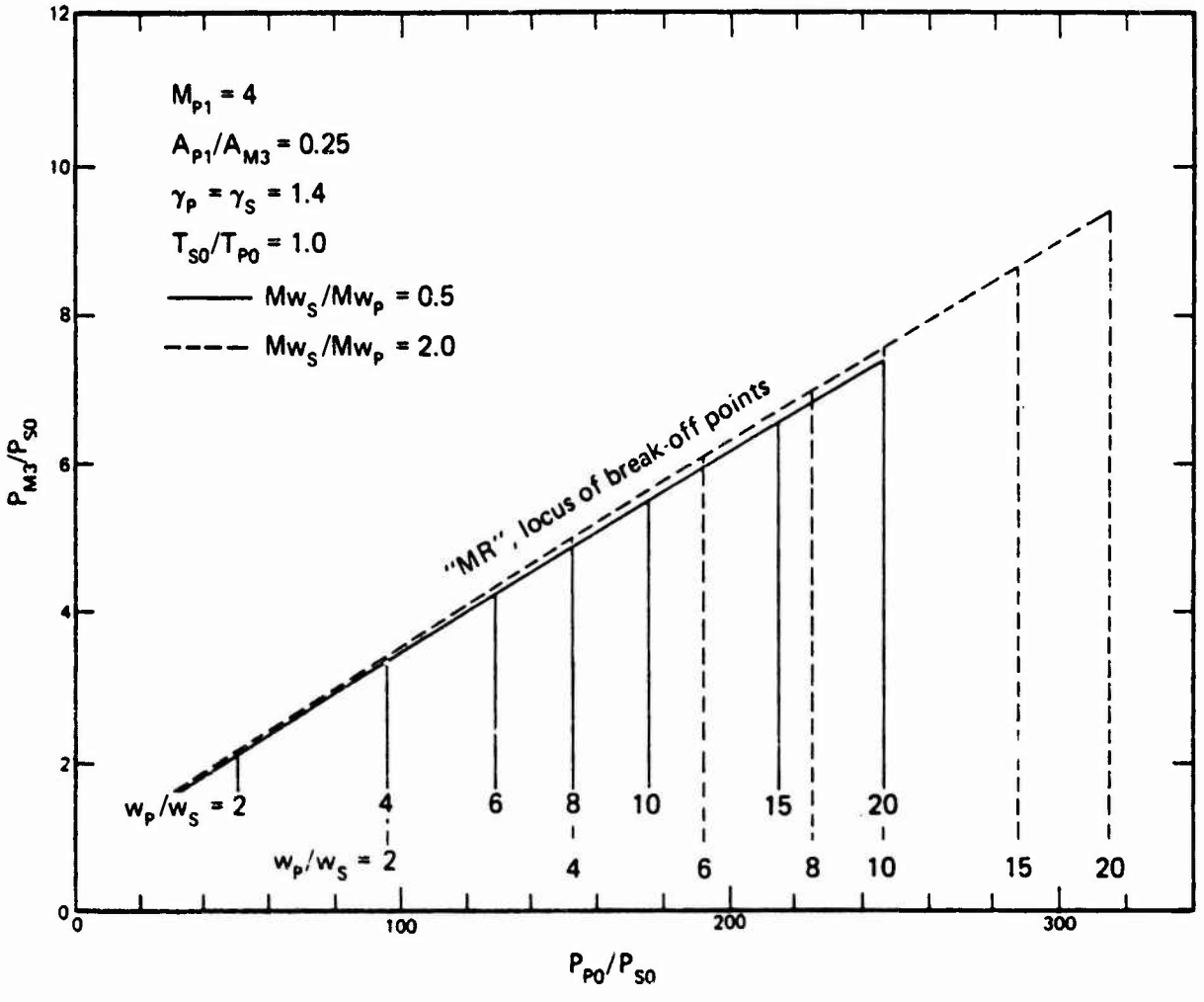


(c) Compression characteristics for parametric variations in $Mw_S/Mw_P$

Figure 2.3-4 Continued

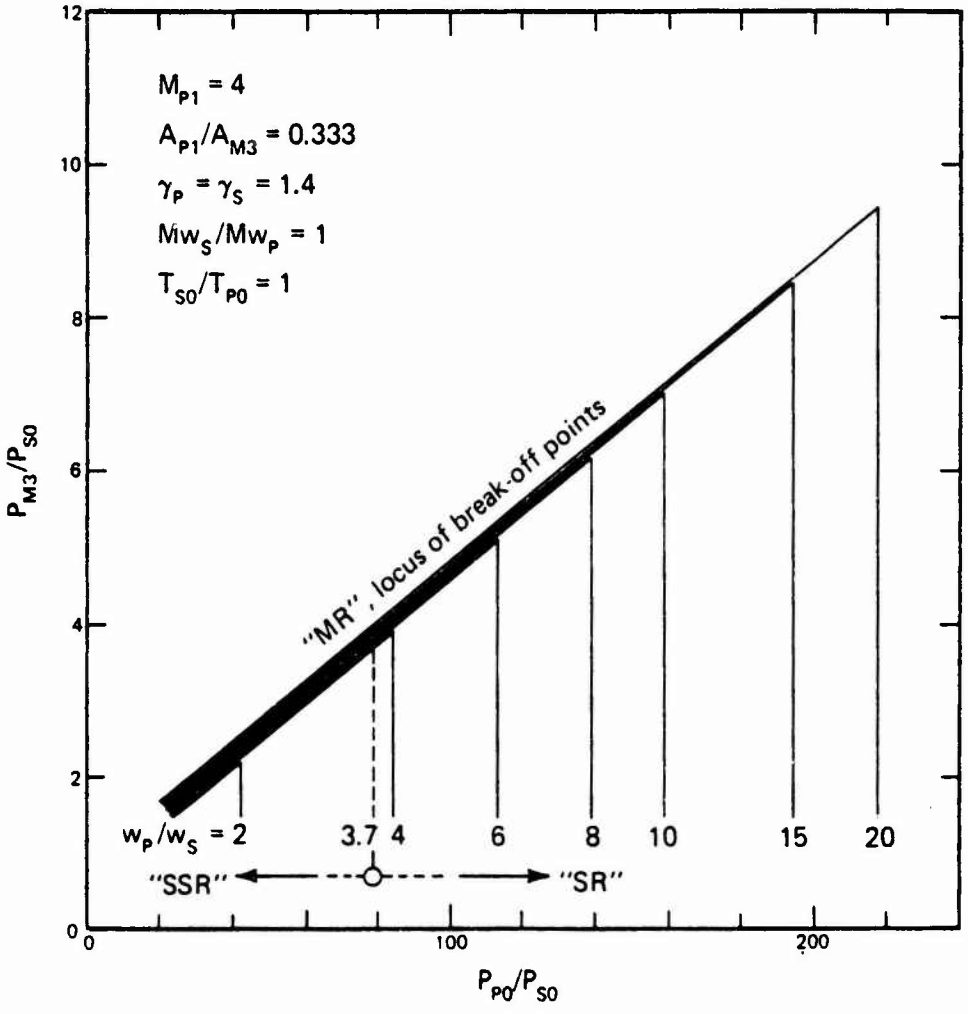


(d) Compression characteristics for a variation in $A_{P1}/A_{M3}$

Figure 2.3-4 Continued

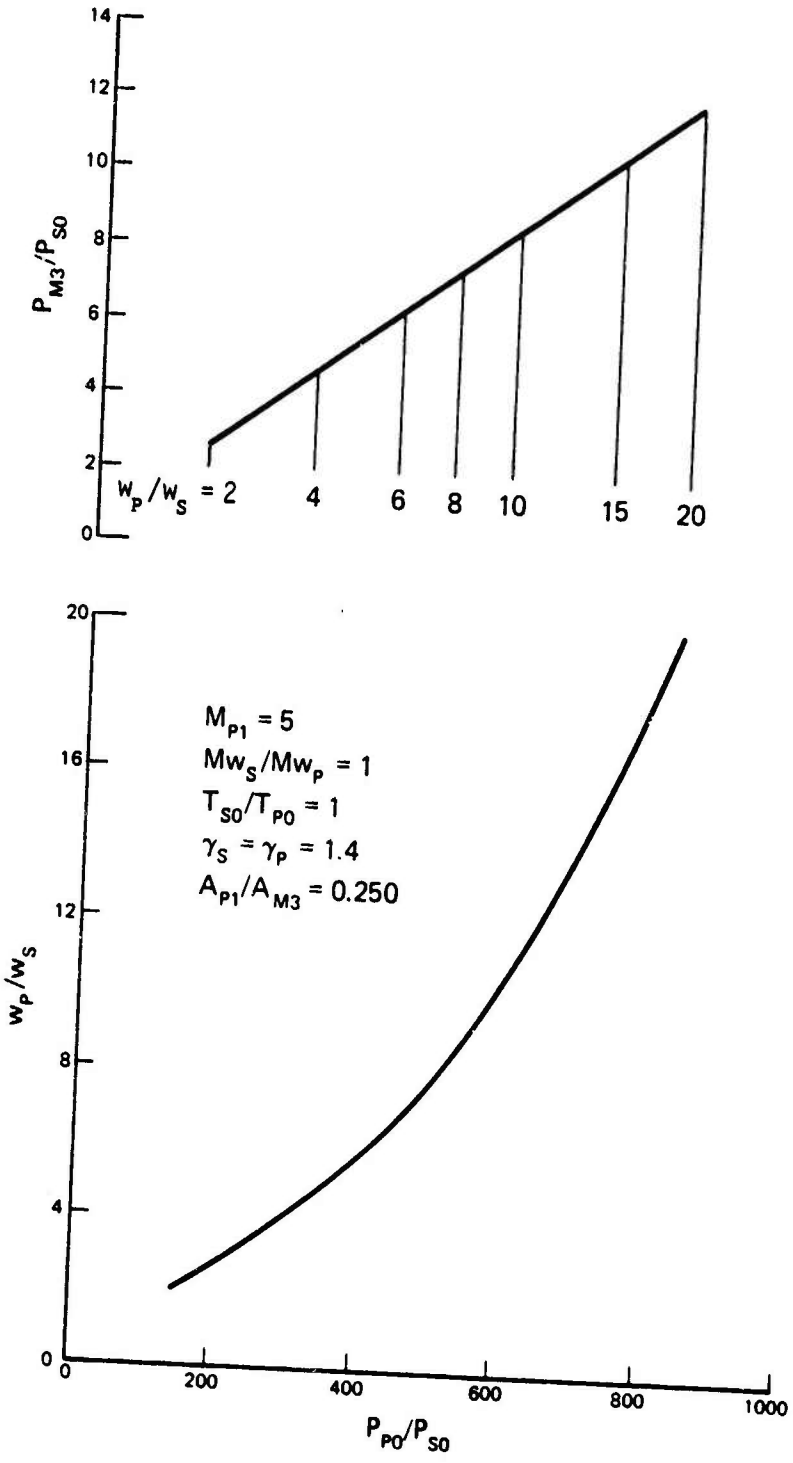


(e) Mass flow and compression characteristics for a variation in $M_{P1}$

Figure 2.3-4 Concluded

Some of the even more simplified analyses of constant area ejectors assume matched static pressures at the confluence of the secondary and primary streams, i.e., $P_{S1} = P_{P1}$. For the configuration analyzed in Fig. 2.3-4(b), the portion of the operating characteristics where this is true is indicated by the dotted band. The range is seen to be rather limited and thus does not present a complete picture of the overall ejector operating characteristics. As a consequence, one must conclude that this assumption is overly restrictive and not that useful.

Figures 2.3-4(c,d,e) show the effects of variations in $Mw_S/Mw_P$, $A_{P1}/A_{M3}$, and $M_{P1}$, respectively, on the compression characteristics of these constant-area ejectors.

## 2.4 STAGED CONSTANT-AREA EJECTOR SYSTEM

When an application requires an ejector system to have an overall compression-pressure ratio greater than 7-10, considerations of optimization, operating pressure levels, mass flowrate ratio, etc., indicate that a multi-staged ejector system should be used. In staged ejector systems, each stage must pump <u>all</u> of the mass flow through the preceding stages unless interstage condensation is used. If interstage condensation is not practical, the size and total primary mass flowrate requirements effectively limit, except in very special cases, the number of ejector stages to two. For purposes of demonstration, a two-stage ejector system based on the constant-area ejector will be discussed.

### 2.4.1 System configuration

A block diagram of a staged ejector system is shown in Fig. 2.4-1. The overall compression ratio and mass flowrate ratio are

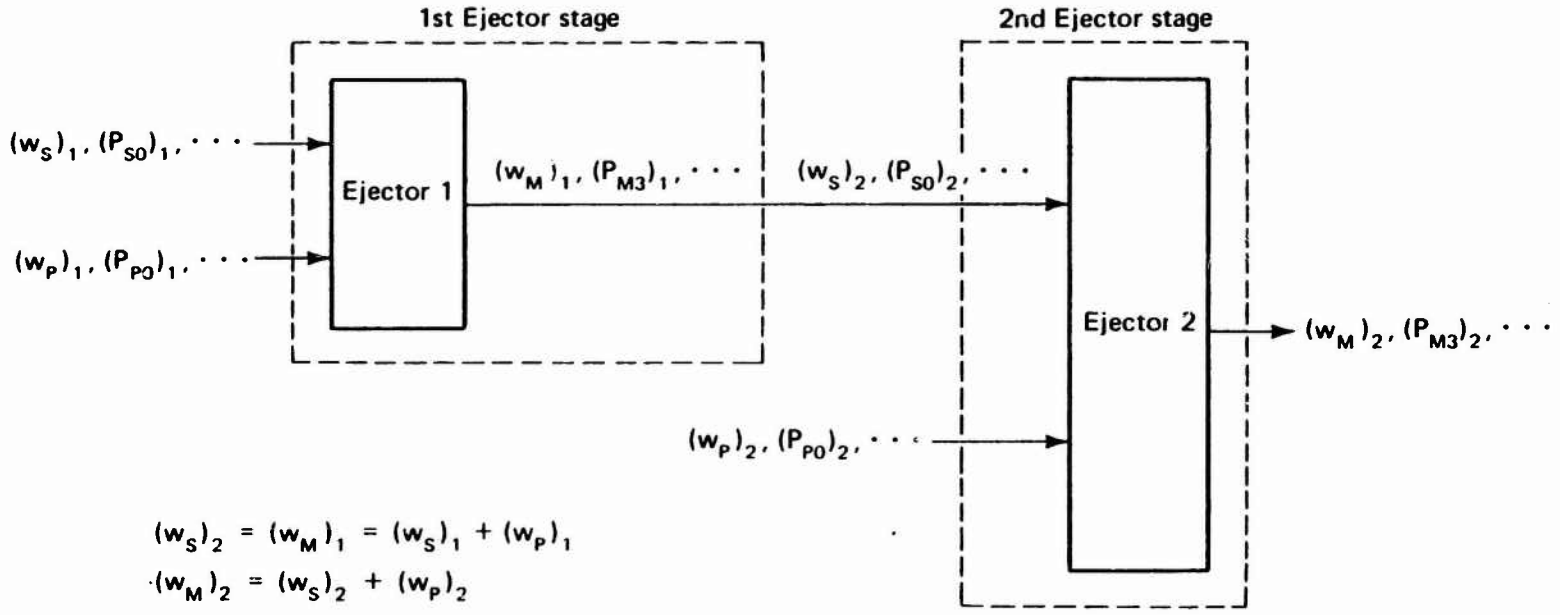


Figure 2.4-1 Staged ejector configuration and notation

of principal concern; for each stage, the primary-to-secondary pressure ratio is also of interest. These system characteristics, referring to Fig. 2.4-1, can be expressed in terms of the individual stages by the following equations.

$$\frac{(w_s)_1}{(w_p)_T} = \frac{(w_s/w_p)_1}{\{1 + [1 + (w_s/w_p)_1]/(w_s/w_p)_2\}} \tag{2.4-1}$$

where $(w_p)_T = (w_p)_1 + (w_p)_2$. The overall compression ratio is

$$\frac{(P_{M3})_2}{(P_{s0})_1} = \left(\frac{P_{M3}}{P_{s0}}\right)_2 \cdot \frac{(P_{s0})_2}{(P_{M3})_1} \cdot \left(\frac{P_{M3}}{P_{s0}}\right)_1 . \tag{2.4-2}$$

The pressures, $(P_{s0})_2$ and $(P_{M3})_1$, are related by the diffuser linking the first-stage exit and the second-stage stagnation chamber; for the purposes of this example, a value of 90% of the isentropic pressure rise, $r_d = 0.90$, will be assumed. That is,

$$\frac{(P_{s0})_2}{(P_{M3})_1} = r_d \left(\frac{P_{M0}}{P_{M3}}\right)_1 . \tag{2.4-3}$$

The individual stage operating pressure ratios are $(P_{P0}/P_{s0})_1$ and $(P_{P0}/P_{s0})_2$; the second-stage pressure ratio can be expressed in terms of the first-stage pressure ratio by

$$\frac{(P_{P0})_2}{(P_{s0})_1} = \left(\frac{P_{P0}}{P_{s0}}\right)_2 \cdot r_d \left(\frac{P_{M0}}{P_{M3}}\right)_1 \cdot \left(\frac{P_{M3}}{P_{s0}}\right)_1 . \tag{2.4-4}$$

The next step in the process is to select the operating points of the ejector stages. Loth [7,8] has discussed optimization of staged ejector systems; a relative optimum can be achieved by operating each stage at the same compression ratio and at its break-off point for the given compression ratio. With this stipulation, the individual-stage compression ratio, from Eqs. (2.4-2) and (2.4-3),

$$\left(\frac{P_{M3}}{P_{S0}}\right)_{1,2} = \left[\frac{(P_{M3})_2/(P_{S0})_1}{r_d\,(P_{M0}/P_{M3})_1}\right]^{1/2} \quad . \qquad (2.4\text{-}5)$$

For this example, the specifications for each stage are identical in non-dimensional form. These specifications are summarized in Table 2.4-1; also, note that an overall compression ratio of 7.6 was assumed for this system.

Table 2.4-1
Ejector specifications

| Variable | Value |
|---|---|
| $(\gamma_S)_{1,2}$ | 1.405 |
| $(\gamma_P)_{1,2}$ | 1.405 |
| $(Mw_S/Mw_P)_{1,2}$ | 1.0 |
| $(T_{S0}/T_{P0})_{1,2}$ | 1.0 |
| $(A_{P1}/A_{M3})_{1,2}$ | 0.25 |
| $(P_{M3})_2/(P_{S0})_1$ | 7.6 |
| $(M_{P1})_{1,2}$ | 4.0 |

Using program CAE, the individual stage compression ratio is found from Eq. (2.4-5) to be approximately

$$\left(\frac{P_{M3}}{P_{S0}}\right)_{1,2} = 2.68 \ ;$$

the remainder of the operating characteristics for the staged ejector are given in Table 2.4-2.

Thus, a comparison of the values in Table 2.4-2 shows that some gains can be made by staging. The two-stage ejector in the above example requires approximateiy 39% less primary mass flow and about 16% less

maximum primary pressure. However, in a broader view these gains might not be significant when consideration is given to the additional hardware required. Also, a more nearly optimum single-stage ejector could, in all probability, be found for this application.

Table 2.4-2
Single and staged ejector performance comparison

| Variable | Value |
|---|---|
| (1) Two-staged ejector | |
| $(w_s/w_p)_{1,2}$ | 0.47 |
| $(P_{M3}/P_{s0})_{1,2}$ | 2.67 |
| $M_{M3}$ | 0.497 |
| $(P_{p0}/P_{s0})_{1,2}$ | 68 |
| $(P_{p0})_2/(P_{s0})_1$ | 194 |
| $(P_{M3})_2/(P_{s0})_1$ | 7.6 |
| $(w_s)_1/(w_p)_T$ | 0.114 |
| (2) Single-stage ejector | |
| $(w_s/w_p)$ | 0.082 |
| $(P_{M3}/P_{s0})$ | ~7.6 |
| $M_{M3}$ | 0.43 |
| $(P_{p0}/P_{s0})$ | 231 |

The result of this simple example indicates the need for further and broader parametric studies of the two-stage versus one-stage ejector system.

# 3.0 EXPERIMENTAL INVESTIGATION

A series of cold-flow, air-to-air experiments has been conducted with small scale axisymmetric ejectors. The configurations investigated include:

(1) constant-area ejectors,

(2) variable-area ejectors, and

(3) slotted-nozzle ejectors.

The experiments provide a data base for comparison with the theory developed in the preceding section and they also provide information on the details of the ejector flowfields which cannot be predicted with the simplified models.

Descriptions of the experimental apparatus and procedure and discussions of the results are contained in the following sections.

## 3.1 COLD-FLOW, AIR-TO-AIR, EJECTOR EXPERIMENTS

### 3.1.1 Experimental apparatus and procedure

The small-scale ejector apparatus is illustrated in Figs. 3.1-1 through 3.1-6. Figure 3.1-1 is a photograph of the continuous flow facility with the axisymmetric ejector and secondary, mass flow measurement section installed. Also visible are the test stands, control panel, and manometer bank. A second photograph of the axisymmetric ejector is presented in Fig. 3.1-2 with the three mixing tubes used in the experimental investigation. An additional schematic view of the axisymmetric ejector design is given in Fig. 3.1-3.

The cold-flow, small-scale experiments were conducted with each of the interchangeable, primary nozzles (M = 2 conical nozzle, M = 2.5

Figure 3.1-1 Continuous flow facility with axisymmetric ejector and secondary, mass flow measurement section installed.

Figure 3.1-2 Axisymmetric ejector with (left to right) variable-area mixing tube with diffuser; 1.245 in. I.D. constant-area mixing tube installed; and 0.995 in. I.D. constant-area mixing tube

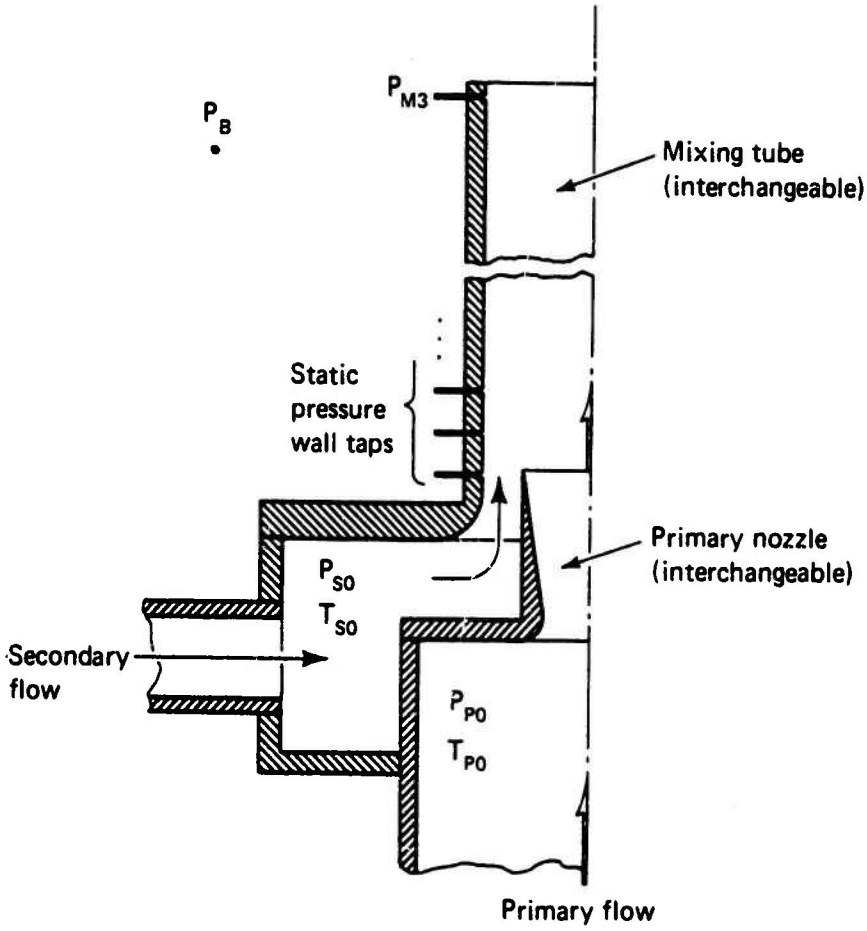


Figure 3.1-3 Schematic of axisymmetric ejector configuration

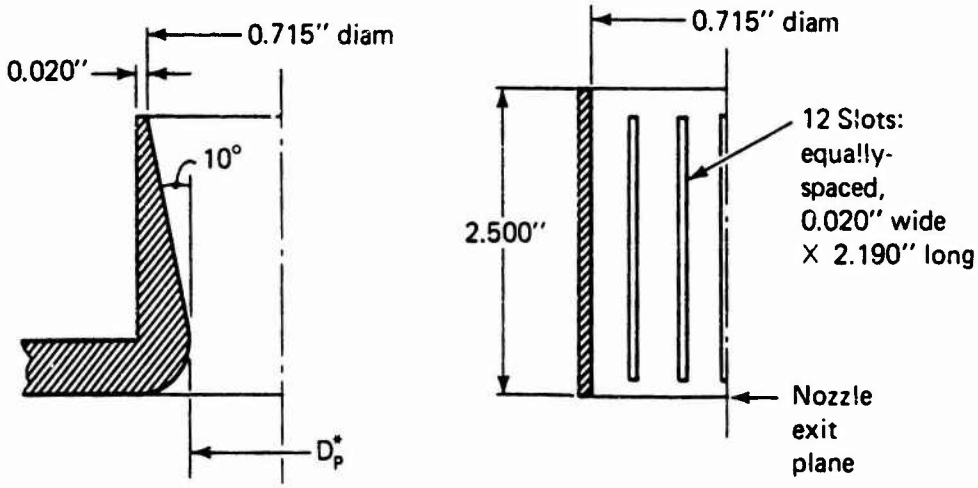


(a) *Basic conical nozzle.*

(b) *Slotted extension for nozzle.*

| Nozzle | $M_{P1}$ | $D_p^*$ in. |
|---|---|---|
| 1 | 2.0 | 0.550 |
| 2 | 2.5 | 0.440 |
| 3* | 2.5 | 0.440 |
| *Slotted nozzle | | |

(c) *Nozzle specifications.*

Figure 3.1-4 Schematics and specifications of ejector primary nozzles

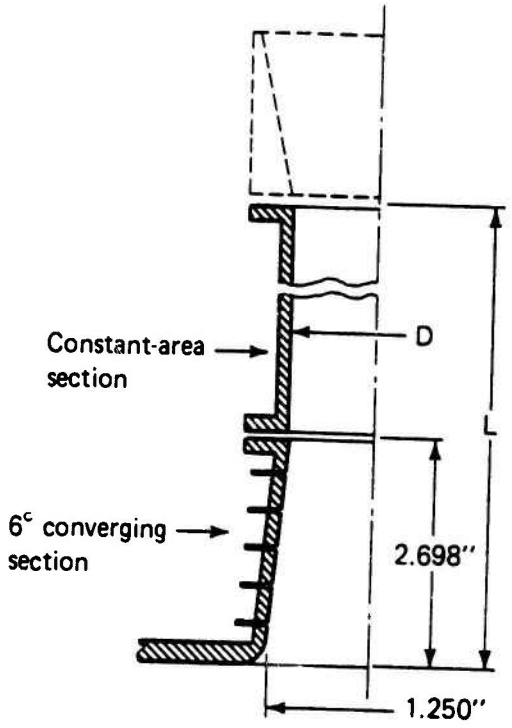


(a) *Variable-area mixing section.*

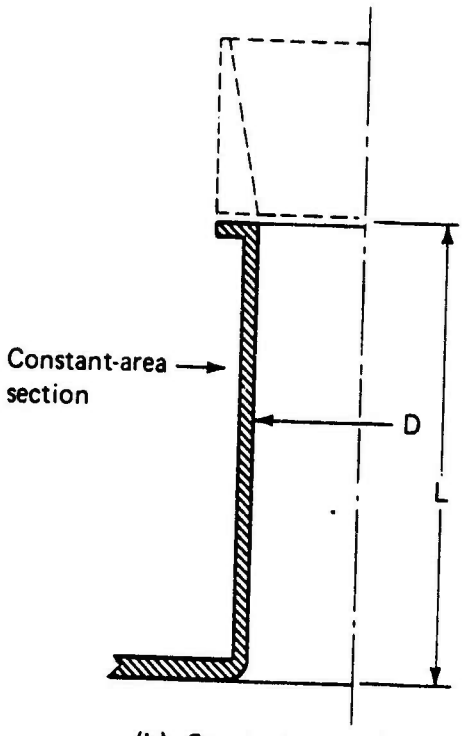


(b) *Constant-area mixing section.*

| Mixing tube | D in. | L in. |
|---|---|---|
| 1 | 0.995 | 12.500 |
| 2 | 1.245 | 13.000 |
| 3* | 0.995 | 12.882 |
| *With 6° converging section | | |

(c) *Mixing section specifications.*

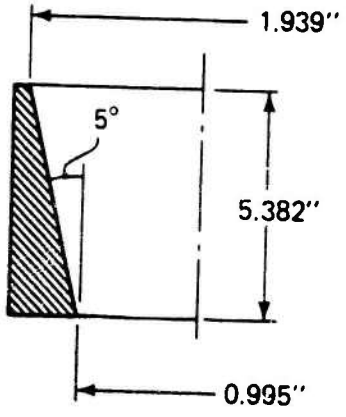


(d) *Subsonic diffuser section.*

Figure 3.1-5 Schematics and specifications of ejector mixing sections

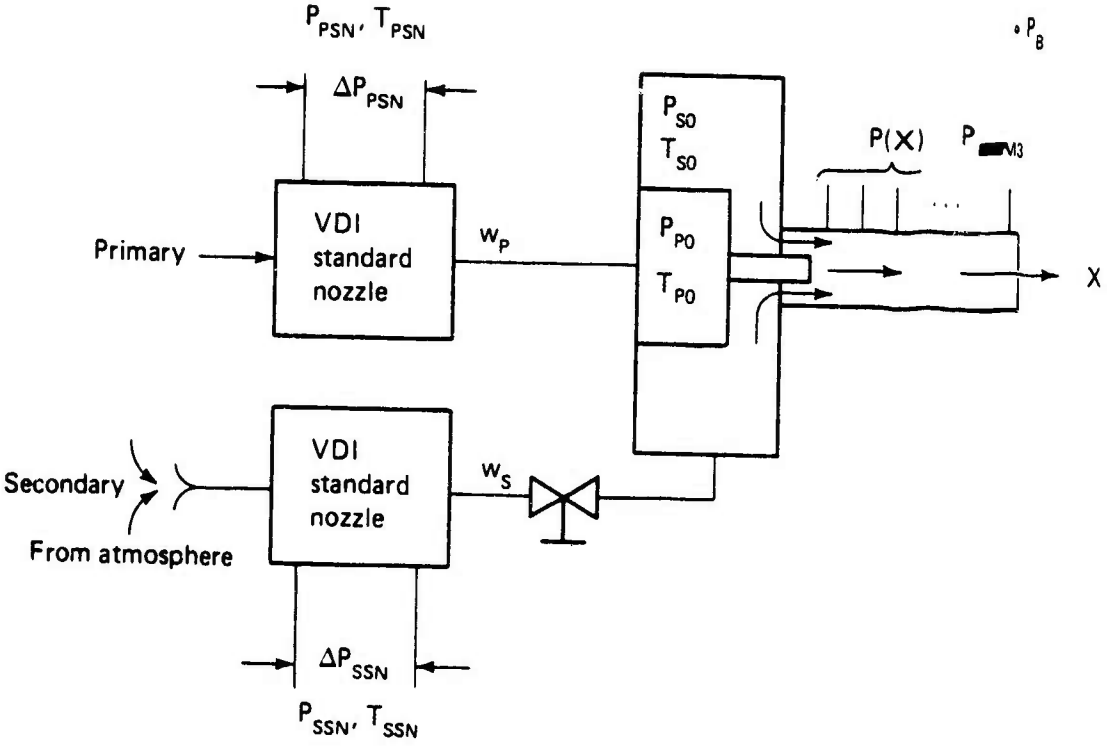


Figure 3.1-6 Experimental ejector set-up and notation

conical nozzle, and M = 2.5 slotted nozzle of Fig. 3.1-4) in combination with each of the interchangeable mixing tubes (1.245 inch I.D. constant-area tube, 0.995 inch I.D. constant-area tube, and variable-area tube of Fig. 3.1-5). The exit area of the primary nozzles was constant providing for identical area ratios $A_{P1}/A_{M3}$ with each mixing tube.

The variable-area mixing tube was constructed such that the entrance diameter was equal to the diameter of the larger 1.245 inch I.D. constant-area tube while the exit diameter was equivalent to the diameter of the smaller 0.995 inch I.D. constant-area tube. Pressure taps were added on a 0.5 inch spacing through the tapered section of the tube for obtaining the wall pressure distribution. The subsonic diffuser of Fig. 3.1-5 was added to the variable-area tube in all cases and to the 0.995 inch I.D. tube in selected tests.

Figure 3.1-6 is a schematic of the test set-up with notation for the ejector and the primary and secondary mass flow measurement sections. Air was used for both the primary and secondary gases in each experiment while $P_{P0}$ was held constant and $P_B = P_{ATM}$; thus, the ratio $P_{P0}/P_B$ or $P_{P0}/P_{ATM}$ was constant. In addition, $w_P$ was constant for each run since the primary flow was choked in the supersonic nozzle and $P_{P0}$ was constant. The secondary stream was drawn from atmosphere; a valve in the secondary flow line was used to change $w_S$ and $P_{S0}$. Hence, $w_S/w_P$ and $P_{S0}/P_{P0}$ were the variables in each experiment. Since the experiments were performed with constant values of $P_{ATM}/P_{P0}$, the experimental results may be thought of as intersections of the three-dimensional operating surfaces, Figs. 2.1-2 and 2.1-3, with planes of $P_{ATM}/P_{P0}$ = constant. Examples of the resulting two-dimensional parametric curves are sketched in Figs. 2.1-4 and 2.1-7.

3.1.2 Experimental results

The experimental results for the M = 2 conical primary nozzle in the 1.245 inch I.D. ($A_{P1}/A_{M3}$ = 0.333) and 0.995 inch I.D. ($A_{P1}/A_{M3}$ = 0.516) constant-area mixing tubes are presented in Figs. 3.1-7 and 3.1-8. Figure 3.1-7 is a plot of $w_S/w_P$ vs $P_{S0}/P_{P0}$. The experimental values lie very close to the theoretical break-off curves† except at very small values of $w_S/w_P$ where, as previously discussed, the flowfield becomes two-dimensional in nature. The compression ratio $P_{ATM}/P_{S0}$ is plotted against $P_{P0}/P_{S0}$ in Fig. 3.1-8. The experimental data points lie below the theoretical break-off curves which simply indicates that the ejector was operating in the $P_{P0}/P_{ATM}$ independent regime.††

Due to the somewhat congested nature of the theoretical $P_{ATM}/P_{S0}$ vs $P_{P0}/P_{S0}$ curves, similar to those shown in Figs. 2.3-4(a-d), the theoretical curves were not completed in the $P_{P0}/P_{ATM}$ independent region of Fig. 3.1-8 except for $w_S/w_P$ = 0.316, 0.108, 0.074, and 0.043 at $A_{P1}/A_{M3}$ = 0.330. Comparisons between the theoretical and experimental results serve to validate the one-dimensional flow model.

From Fig. 3.1-8 it would appear that the ejector was operating closer to the theoretical break-off curve for $A_{P1}/A_{M3}$ = 0.330; however, a vertical line drawn through the experimental data and the theoretical break-off curve to determine the break-off points, indicates different

---

† Recall that the theoretical $w_S/w_P$ vs $P_{S0}/P_{P0}$ curve is invariant and identical to the break-off curve in the $P_{P0}/P_{ATM}$ independent regime.

†† Refer back to Section 2.3 and Fig. 2.3-4 for a more complete presentation of the typical operating characteristics of an ejector system as determined from the theoretical constant-area ejector model.

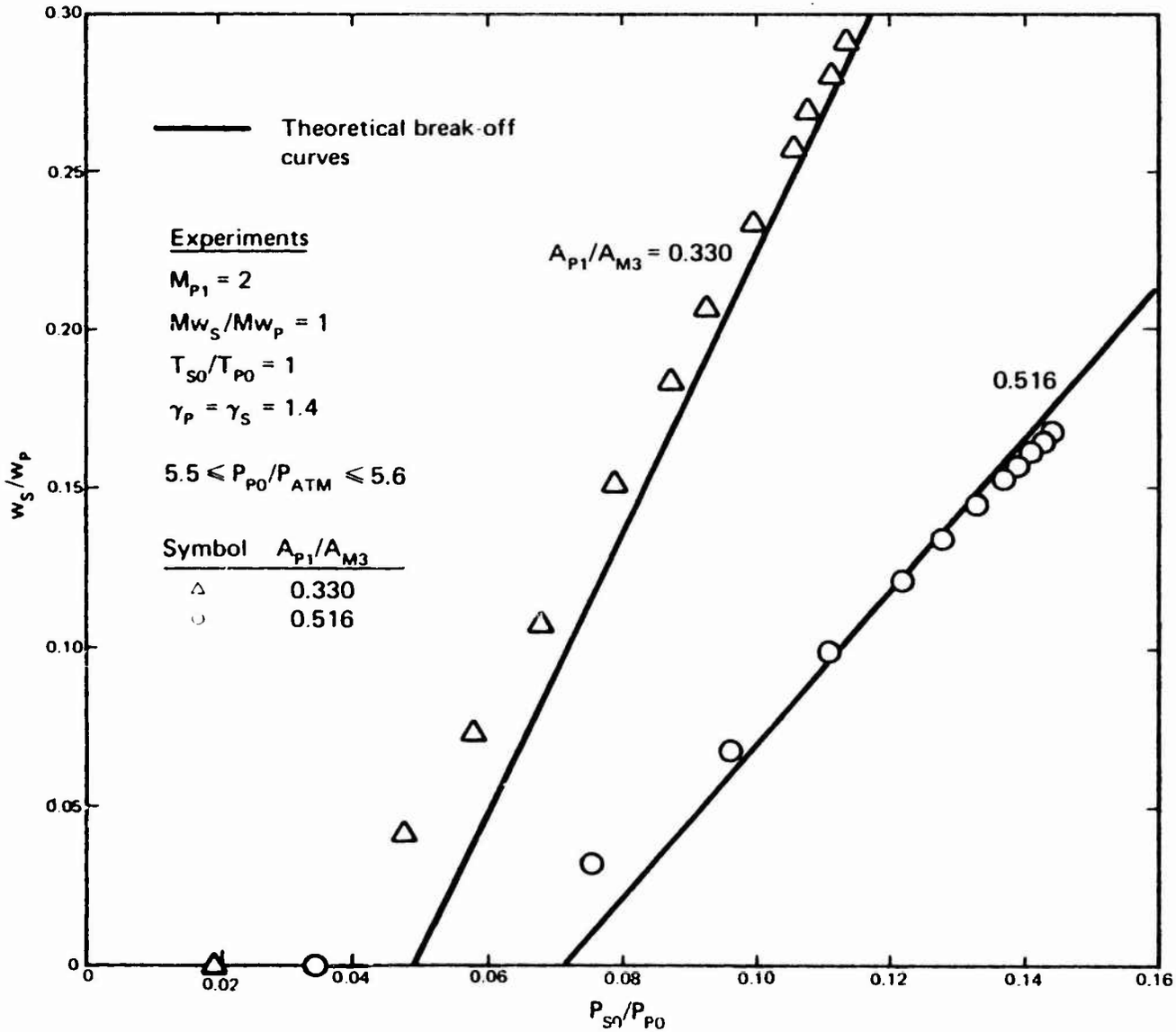


Figure 3.1-7 Constant-area ejector mass flow characteristics ($A_{P1}/A_{M3}$ = 0.330, 0.516 and $M_{P1}$ = 2.0)

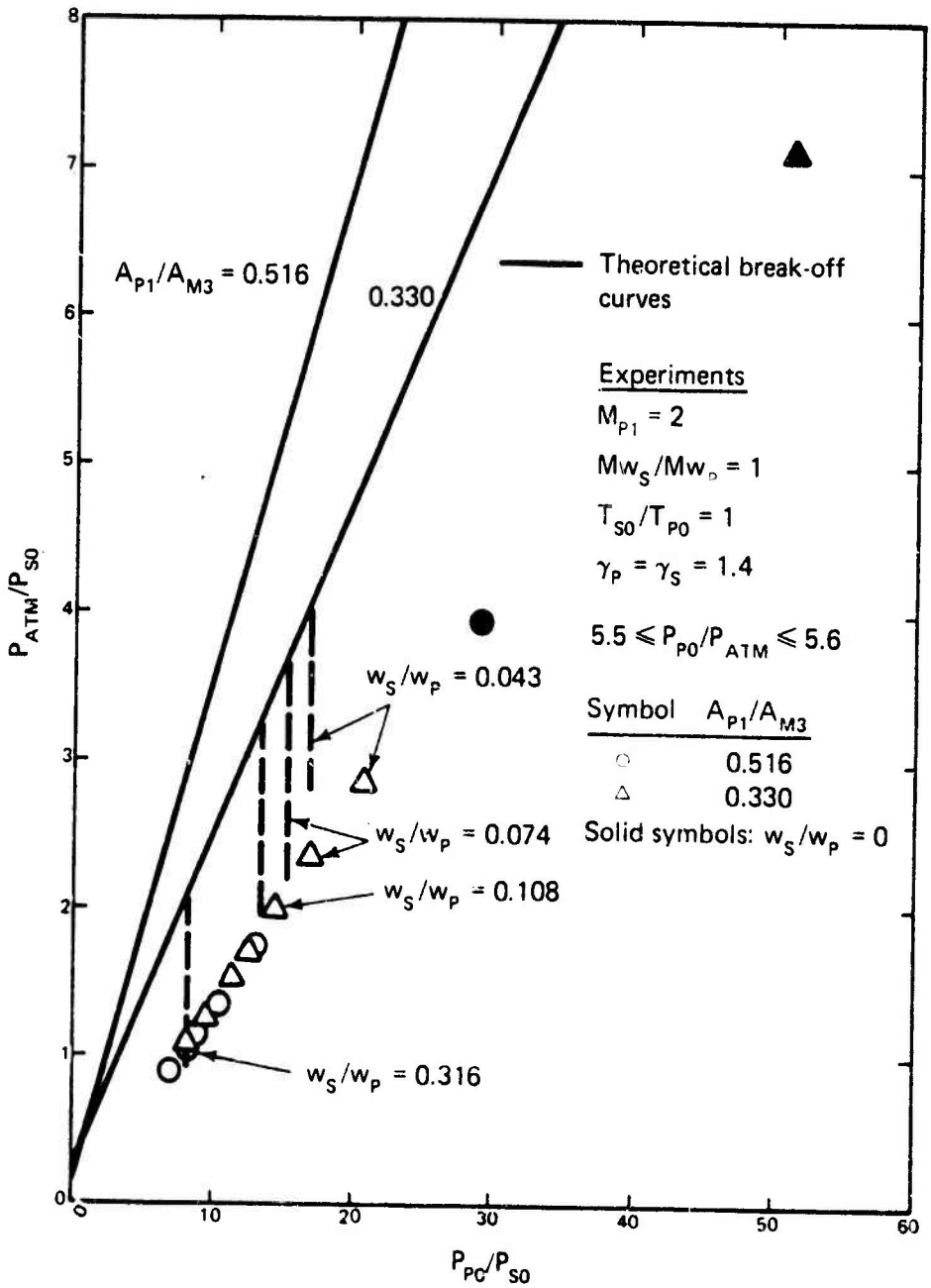


Figure 3.1-8 Constant-area ejector compression characteristics ($A_{P1}/A_{M3}$ = 0.330, 0.516 and $M_{P1}$ = 2.0)

values of $w_S/w_P$ for each area ratio. This fact is borne out by the data points for $w_S/w_P = 0$ at $A_{P1}/A_{M3} = 0.330$ and 0.516; these points indicate that the ejectors were operated significantly below the applicable break-off curve at lower values of $w_S/w_P$.

The experimental results for the M = 2.5 conical primary nozzle in the 1.245 inch I.D. ($A_{P1}/A_{M3} = 0.330$) and 0.995 inch I.D. ($A_{P1}/A_{M3} = 0.516$) constant-area mixing tubes as given in Figs. 3.1-9 and 3.1-10 follow the same trends as for the M = 2 conical nozzle. Again, the experimental values of $w_S/w_P$ vs $P_{SO}/P_{PO}$ are in good agreement with the one-dimensional flow model except at low values of $w_S/w_P$. Since the experimental data points for $P_{ATM}/P_{SO}$ vs $P_{PO}/P_{SO}$ lie below the theoretical break-off curves, ejector operation in the $P_{PO}/P_{ATM}$ independent regime is indicated. Addition of the subsonic diffuser to the 0.995 inch I.D. constant-area tube did not alter the mass flow characteristics of Fig. 3.1-9 since the diffuser affects only the recompression shock structure within the ejector in the $P_{PO}/P_{ATM}$ independent regime. From Fig. 3.1-10 it is apparent that the ejector was operating closer to the theoretical break-off curve with the diffuser; however, the experiment with the diffuser installed was conducted at $P_{PO}/P_{ATM} = 5.5$; whereas, the experiment without the diffuser was performed with $P_{PO}/P_{ATM} = 6.2$. The difference in $P_{PO}/P_{ATM}$, as will be demonstrated below, should have been responsible for the differences in $P_{ATM}/P_{SO}$ values with and without the subsonic diffuser.

The experimental results for the M = 2.5 slotted primary nozzle in the 1.245 inch I.D. ($A_{P1}/A_{M3} = 0.330$) and 0.995 inch I.D. ($A_{P1}/A_{M3} = 0.516$) constant-area mixing tubes are presented in Figs. 3.1-11 and 3.1-12. From Fig. 3.1-11 the experimental data for $w_S/w_P$ vs $P_{SO}/P_{PO}$

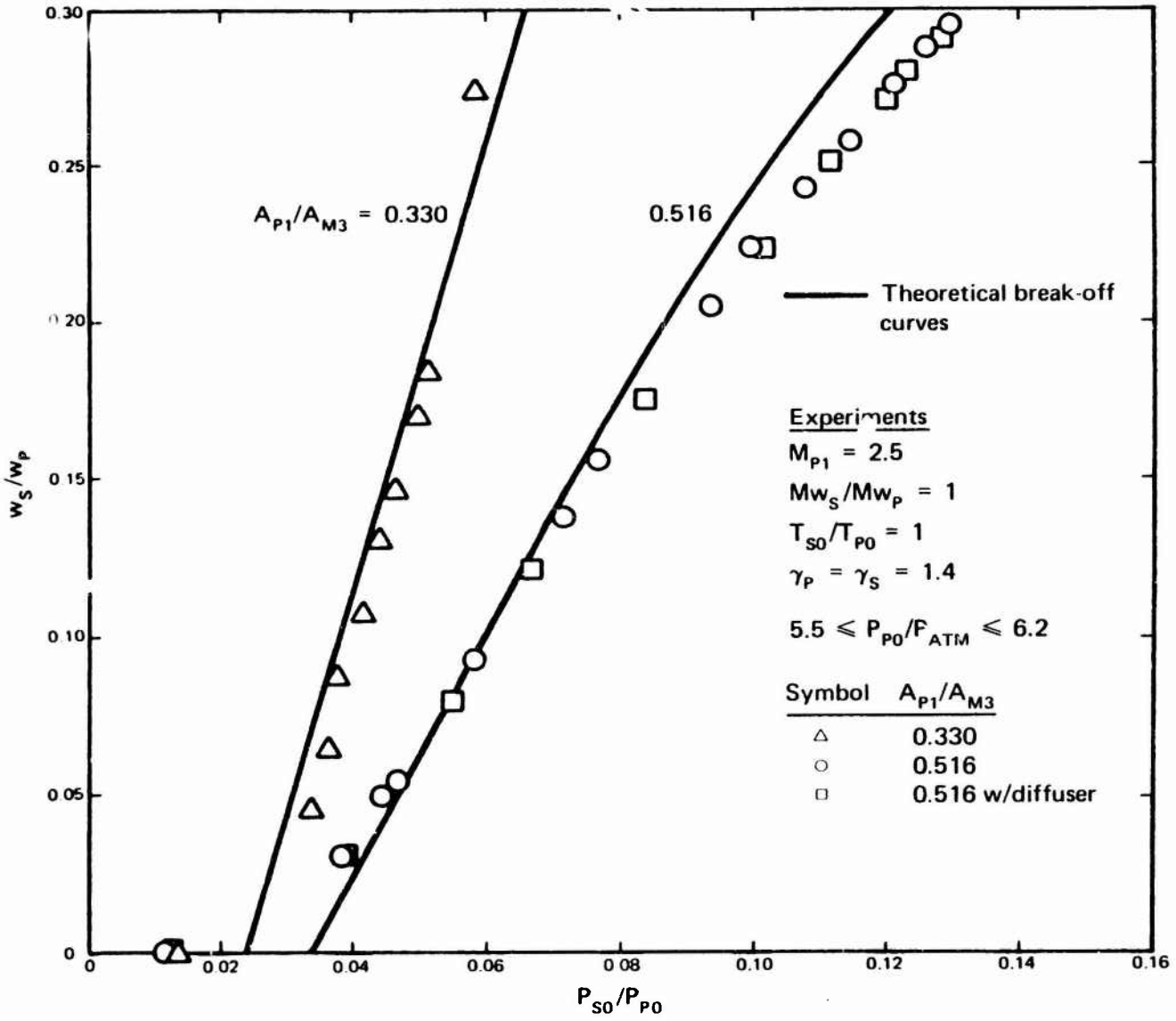


Figure 3.1-9 Constant-area ejector mass flow characteristics ($A_{P1}/A_{M3}$ = 0.330, 0.516 and $M_{P1}$ = 2.5)

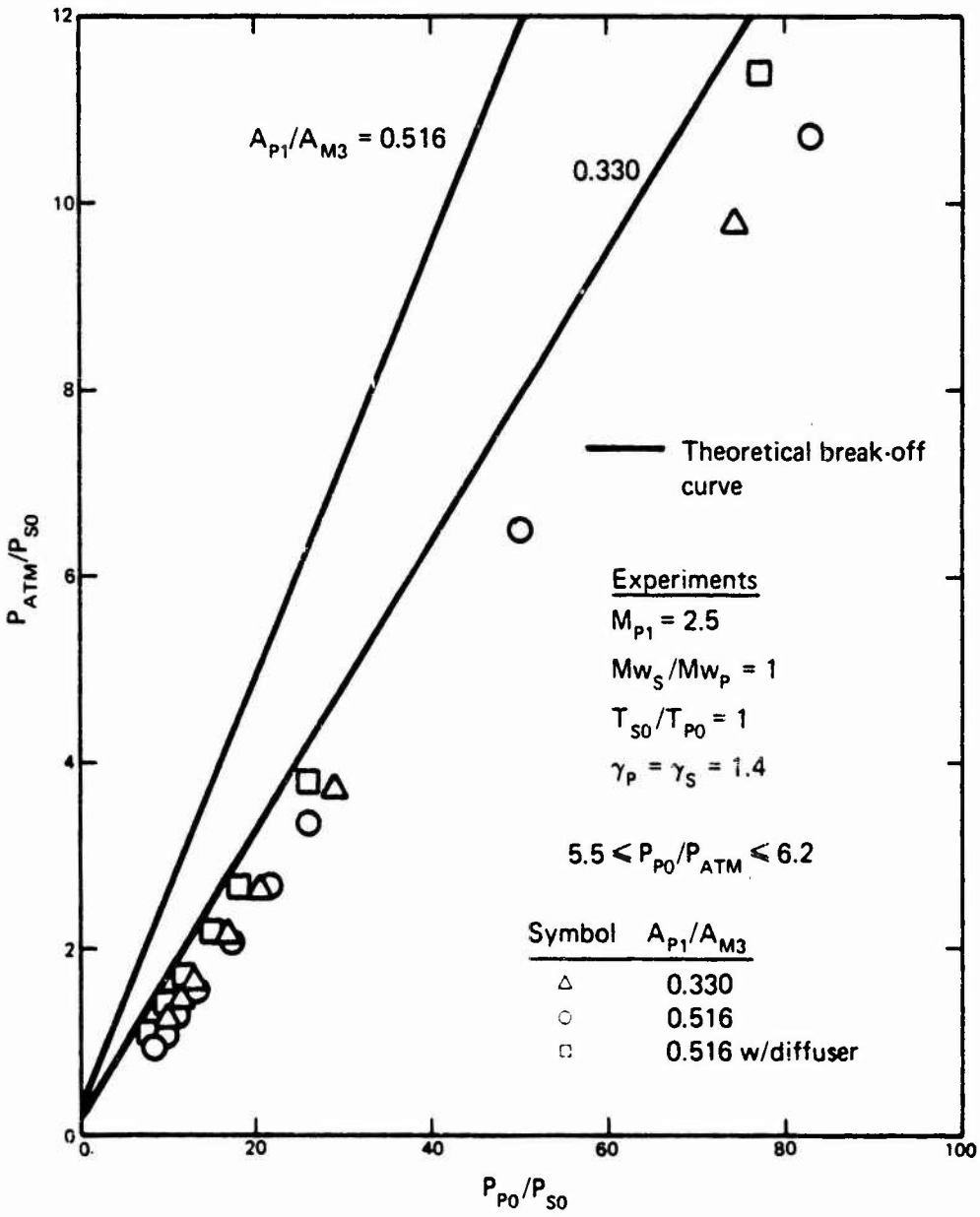


Figure 3.1-10 Constant-area ejector compression characteristics ($A_{P1}/A_{M3}$ = 0.330, 0.516 and $M_{P1}$ = 2.5)

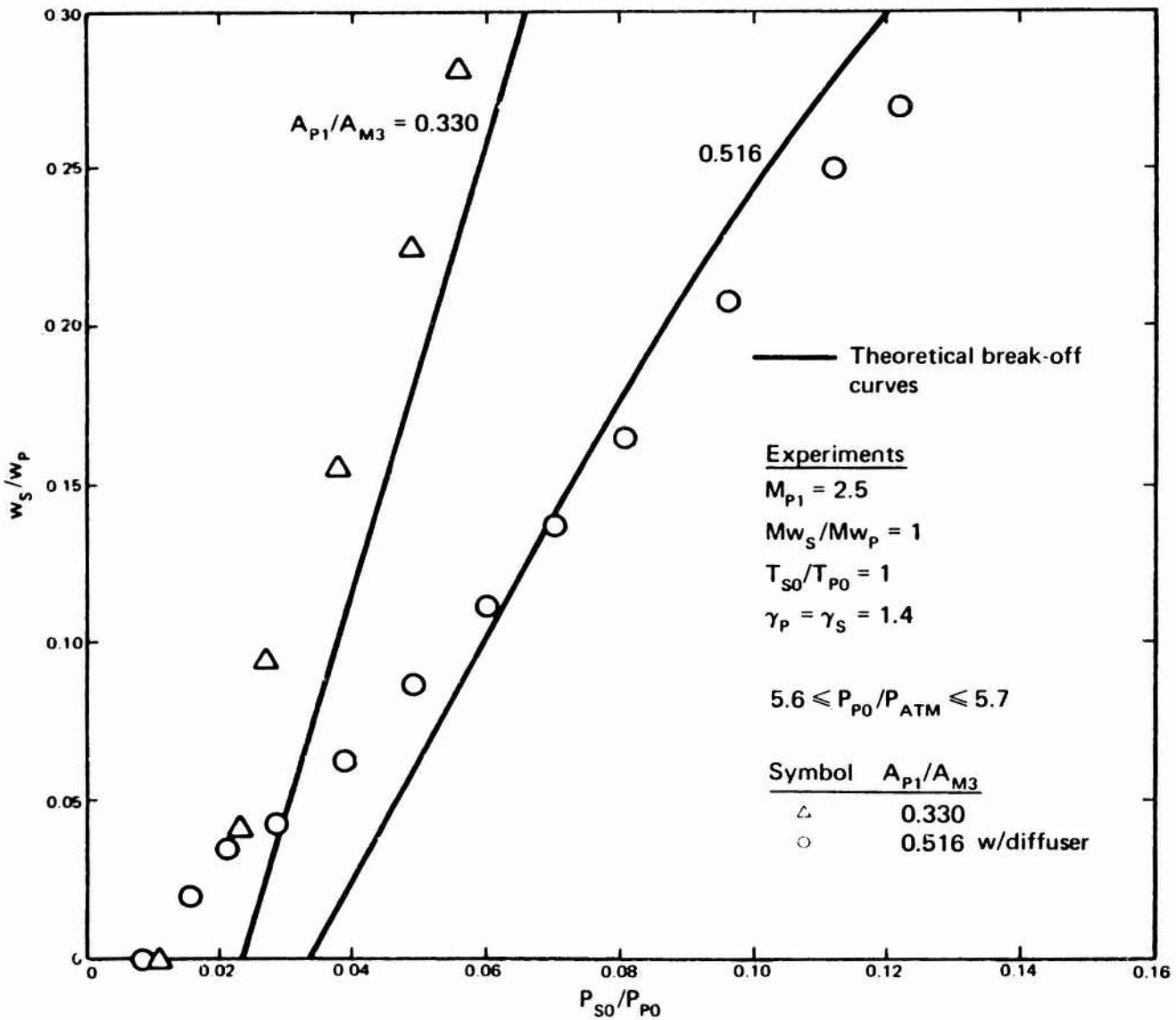


Figure 3.1-11 Constant-area, slotted-nozzle ejector mass flow characteristics ($A_{P1}/A_{M3}$ = 0.330, 0.516 and $M_{P1}$ = 2.5)

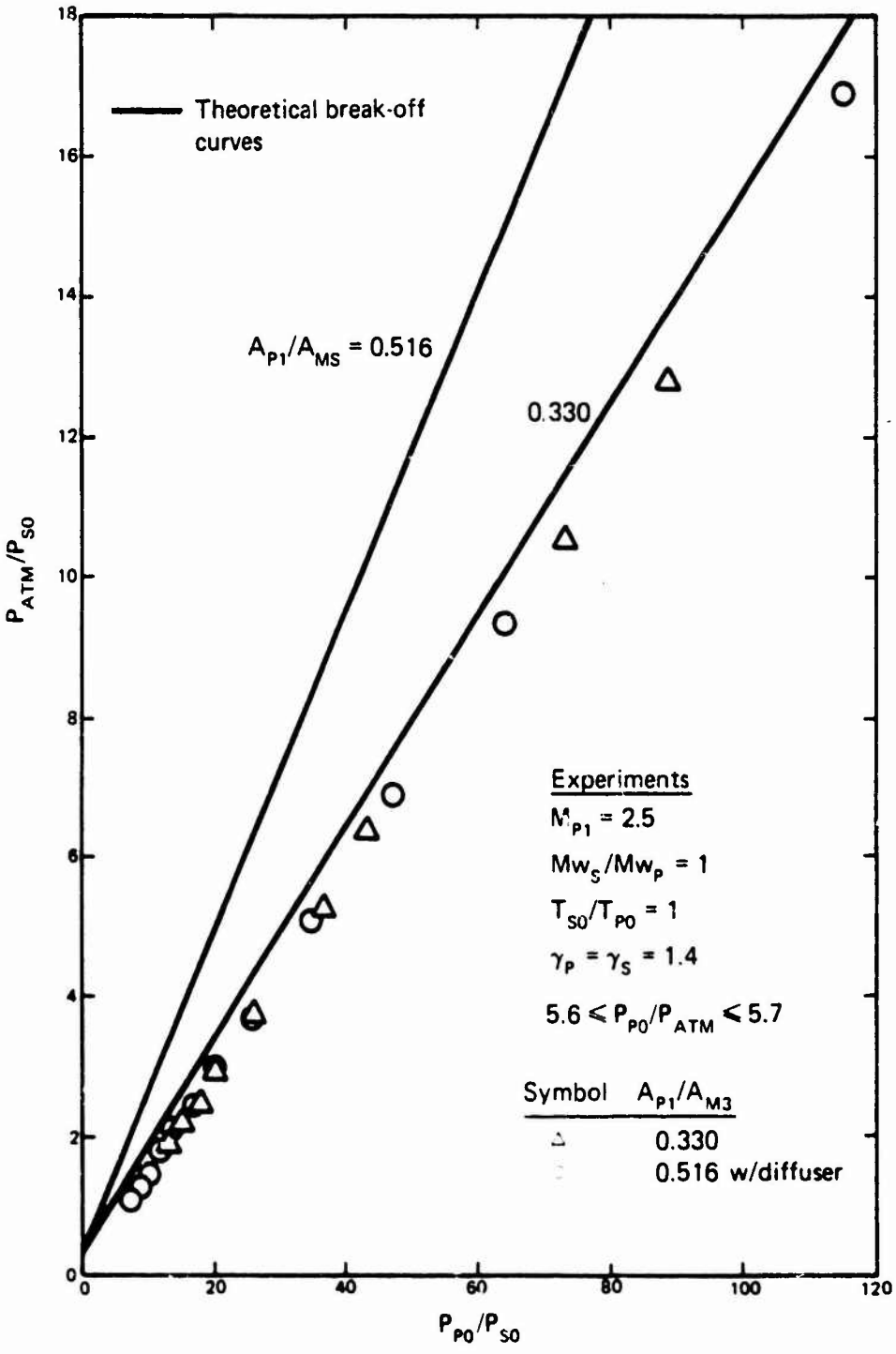


Figure 3.1-12 Constant-area, slotted-nozzle ejector compression characteristics ($A_{P1}/A_{MS}$ = 0.330, 0.516 and $M_{P1}$ = 2.5)

generally follows the theoretical break-off curves. However, deviations from the one-dimensional theory occur at larger values of $w_S/w_P$ than for the M = 2.5 conical nozzle of Fig. 3.1-9, which is not unexpected considering the geometry of the slotted nozzle. The compression ratio data of Fig. 3.1-12 is quite similar to that of Fig. 3.1-10 and indicates that the ejector was operating in the $P_{P0}/P_{ATM}$ independent regime.

The experimental results for the M = 2 and M = 2.5 conical primary nozzles in the variable-area mixing tube† are given in Figs. 3.1-13 through 3.1-18. The theoretical break-off curves are those for an ejector operating under the same conditions but with a constant-area mixing tube of $A_{P1}/A_{M3} = 0.516$. Although the mass flow data of Fig. 3.1-13 deviates from the theoretical break-off curves, the one-dimensional analysis for an area ratio based on the minimum mixing tube area provides a fair representation of variable-area ejector performance, particularly at higher values of $w_S/w_P$. The variation in $P_{P0}/P_{ATM}$ did not alter the mass flow characteristics of Fig. 3.1-13 since the ejector, as shown in Fig. 3.1-14, was always operated in the $P_{P0}/P_{ATM}$ independent regime. Comparison of the compression ratio data of Fig. 3.1-14 shows that the ejector operated closer to the theoretical break-off curves at the lower values of $P_{P0}/P_{ATM}$; this demonstrates the desirability of operating at $P_{P0}/P_B$ values that are near the break-off curve in the independent regime. Note that the dimensionless mass flow characteristics remain unchanged even though the primary stagnation pressure is smaller. Figure 3.1-14

---

†Figure 3.1-5(a) shows this mixing section. The initial entrance diameter is 1.250 inches converging at a wall angle of 6° to a minimum mixing tube diameter of 0.995 inches.

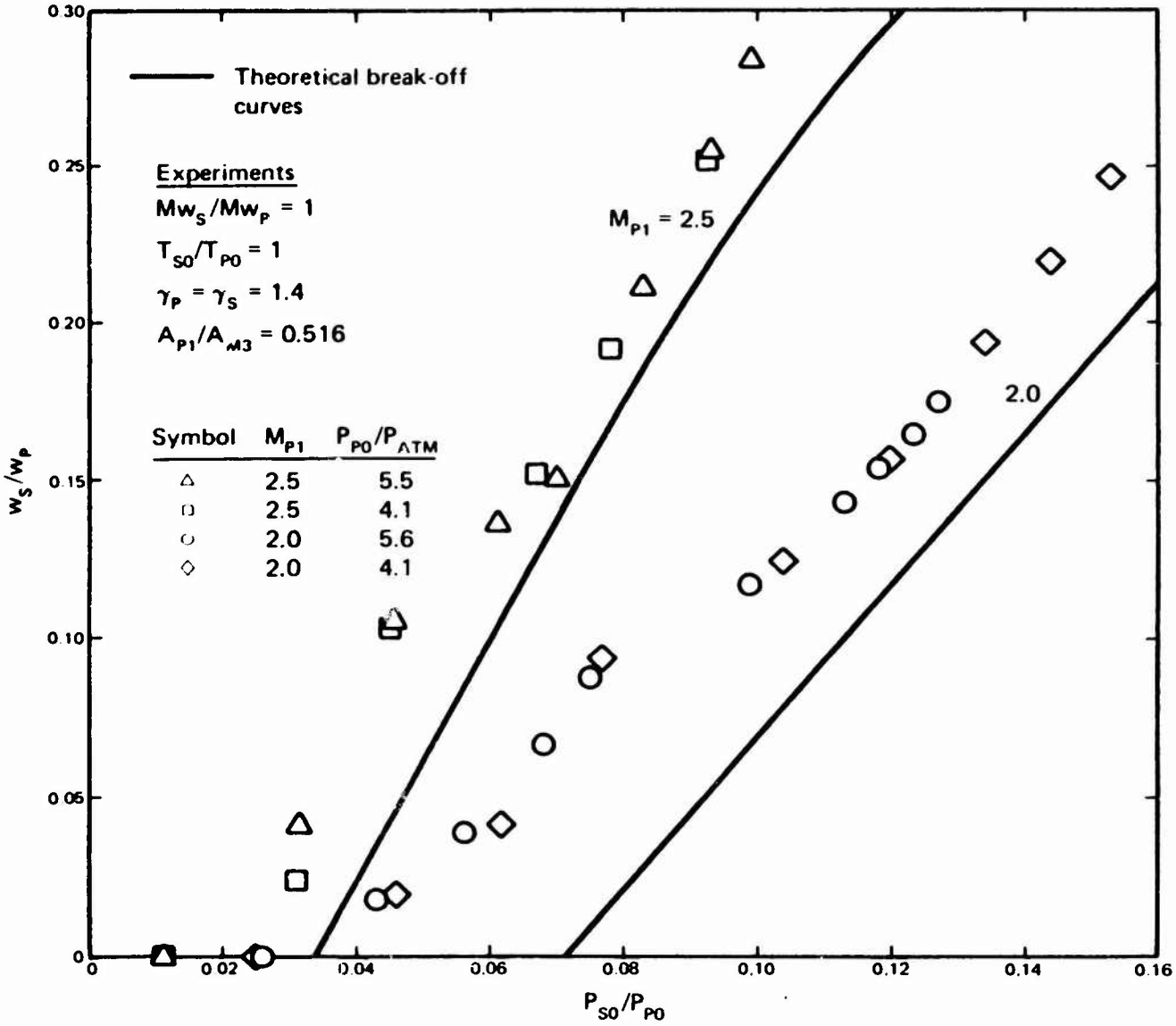


Figure 3.1-13 Variable-area ejector mass flow characteristics ($A_{P1}/A_{M3}$ = 0.516 and $M_{P1}$ = 2.0, 2.5)

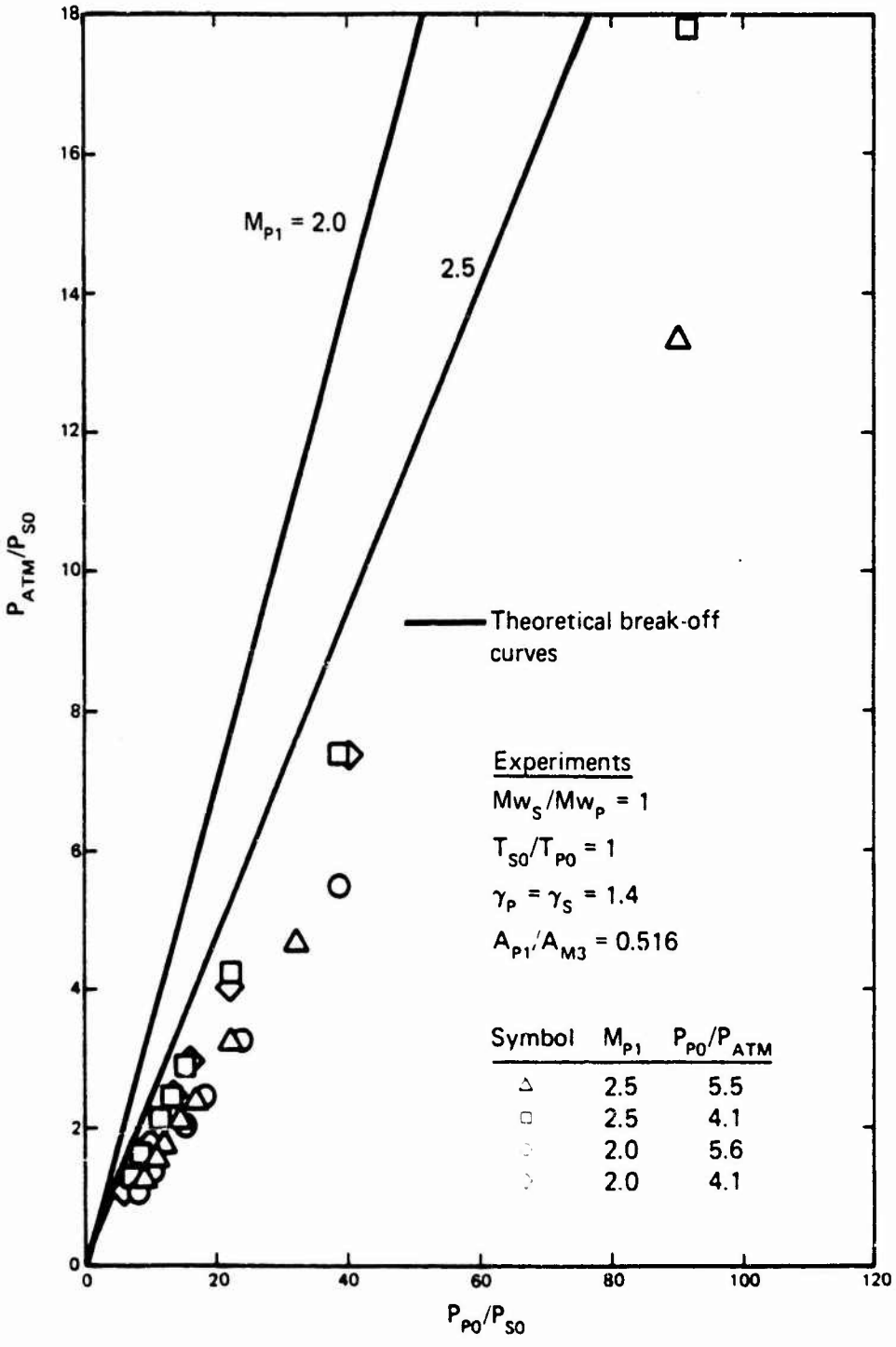


Figure 3.1-14 Variable-area ejector compression characteristics ($A_{P1}/A_{M3}$ = 0.516 and $M_{P1}$ = 2.0, 2.5)

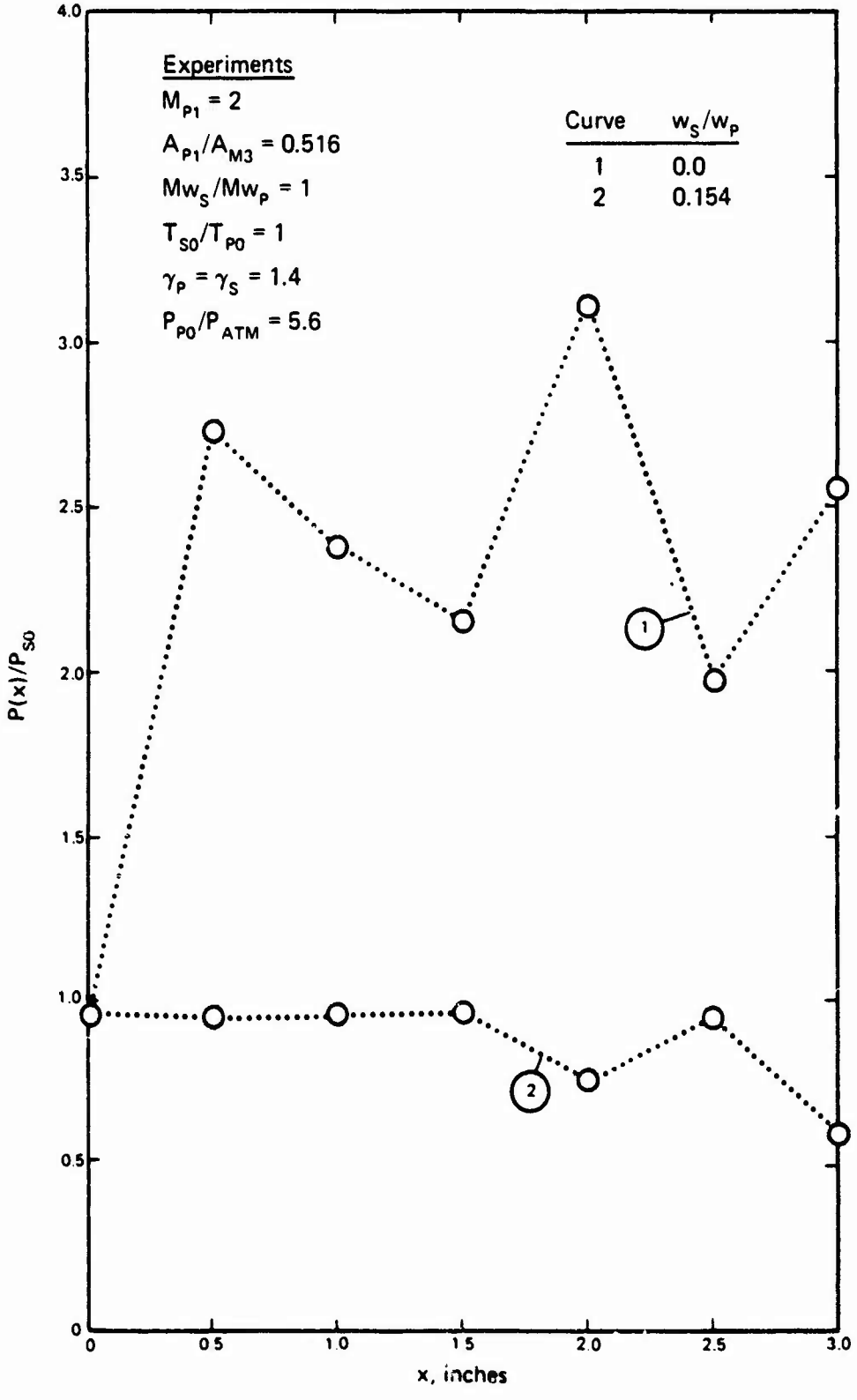


Figure 3.1-15 Variable-area ejector wall pressure distributions ($A_{P1}/A_{M3}$ = 0.516, $M_{P1}$ = 2.0, and $P_{P0}/P_{ATM}$ = 5.6)

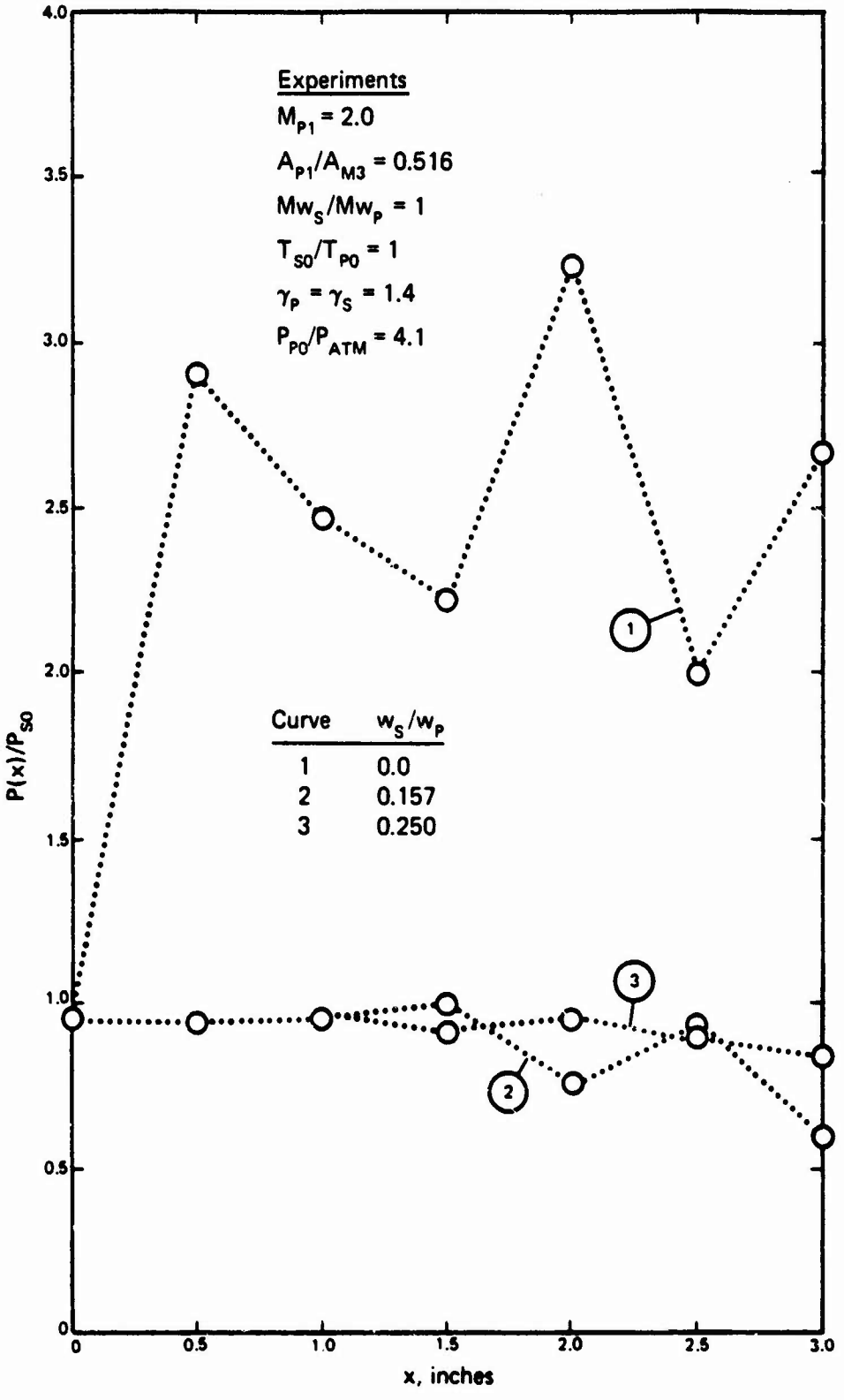


Figure 3.1-16 Variable-area ejector wall pressure distributions ($A_{P1}/A_{M3}$ = 0.516, $M_{P1}$ = 2.0, and $P_{P0}/P_{ATM}$ = 4.1)

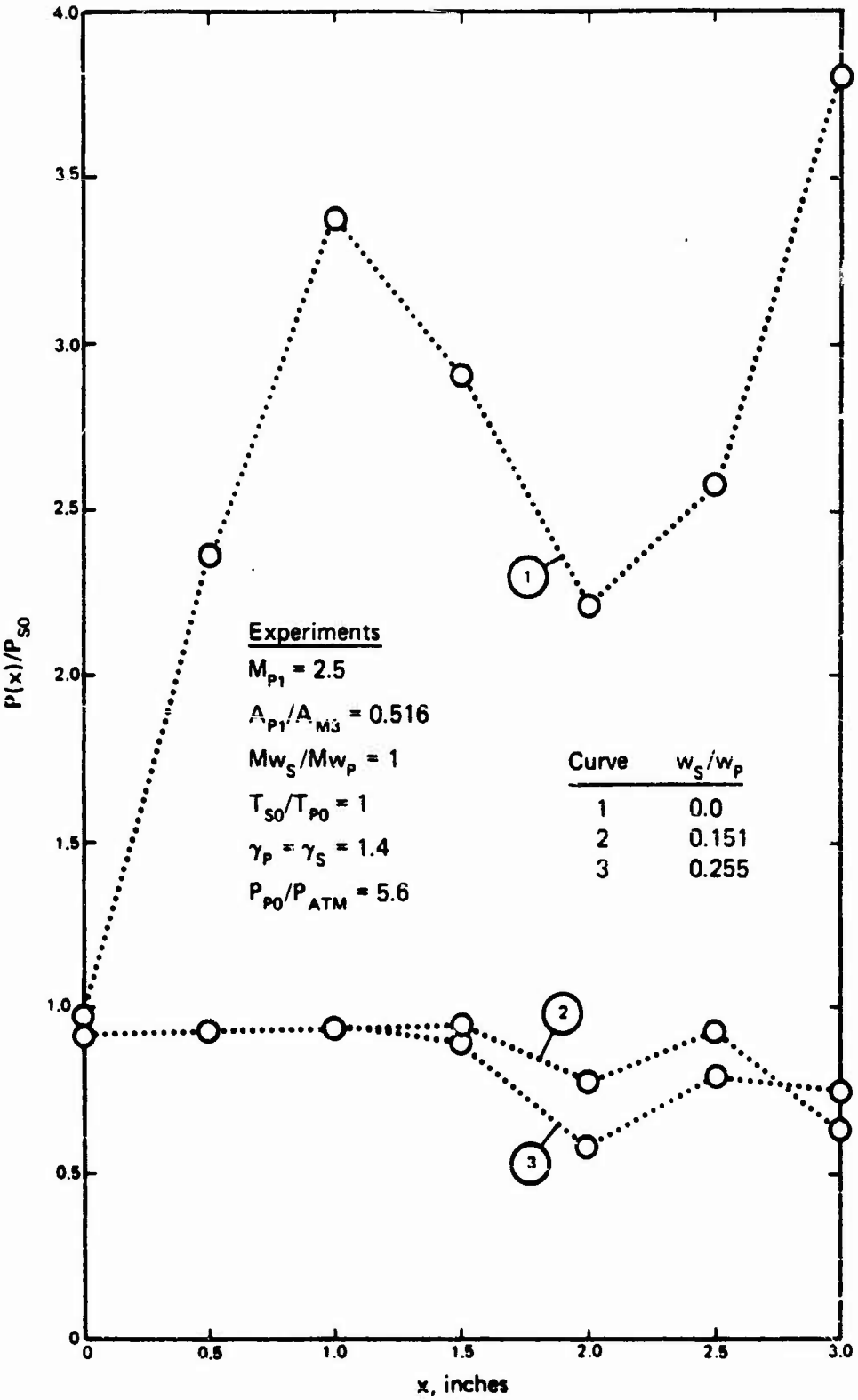


Figure 3.1-17 Variable-area ejector wall pressure distributions ($A_{P1}/A_{M3}$ = 0.516, $M_{P1}$ = 2.5, $P_{P0}/P_{ATM}$ = 5.6)

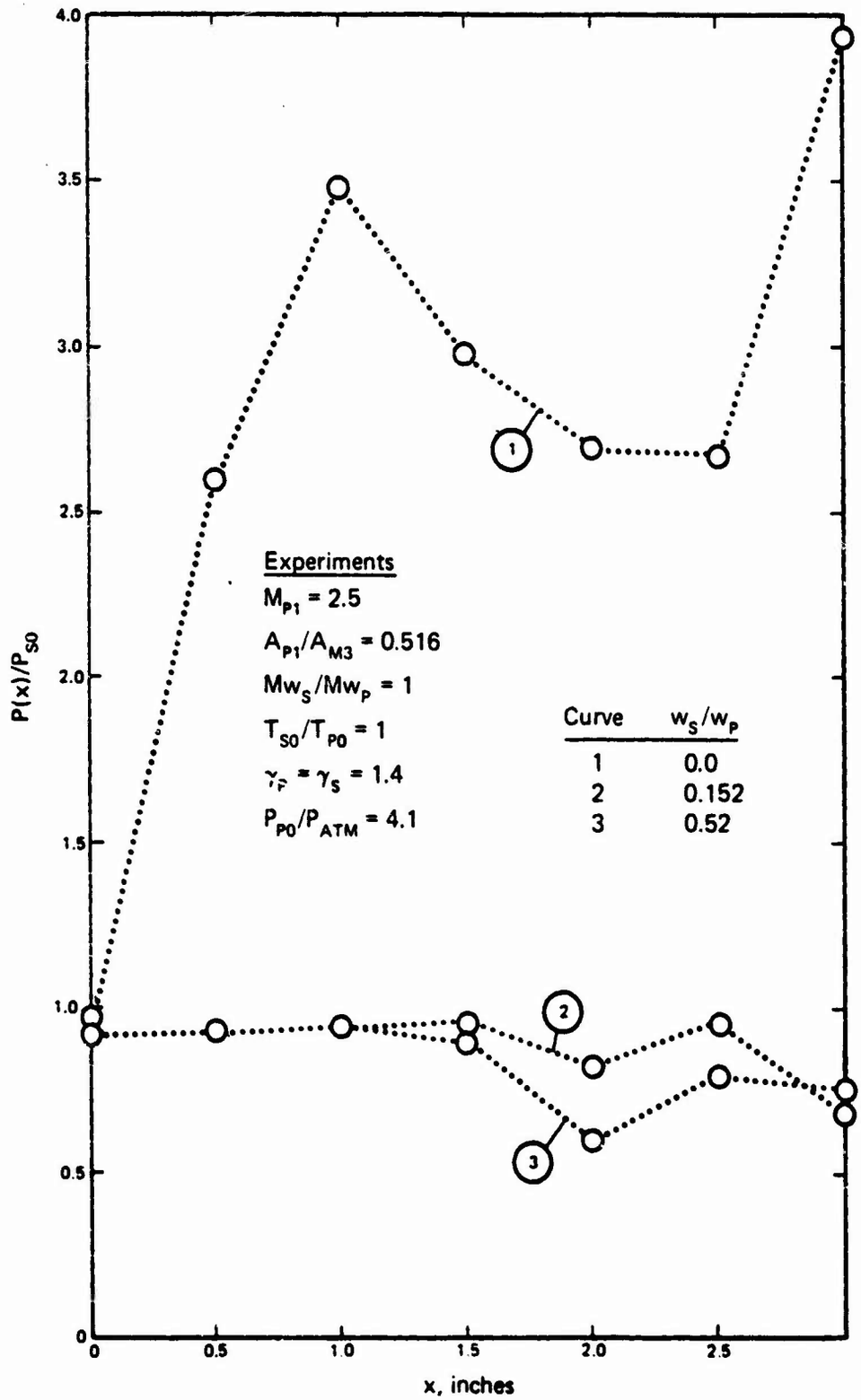


Figure 3.1-18 Variable-area ejector wall pressure distributions ($A_{P1}/A_{M3}$ = 0.516, $M_{P1}$ = 2.5, $P_{P0}/P_{ATM}$ = 4.1)

also shows that the ejector operated closer to the appropriate theoretical break-off curve with the M = 2.5 conical primary nozzle; however, this is due to the fact that for constant $A_{P1}/A_{MS}$, an M = 2.5 nozzle requires a higher value of $P_{PO}/P_{ATM}$ than an M = 2 nozzle for $P_{PO}/P_B$ independent operation. The wall pressure distributions of Figs. 3.1-15 through 3.1-18 show that approximately constant pressure mixing occurred only at higher values of $w_S/w_P$ and, consequently, at lower values of $P_{ATM}/P_{SO}$ with $P_{PO}/P_{ATM}$ differences having little effect. In each of Figs. 3.1-15 through 3.1-18 note that only the initial part of the wall pressure distributions near the primary/secondary confluence are shown and that the final compression is to much higher levels of $P_{ATM}/P_{SO}$.

The experimental results for the M = 2.5 slotted primary nozzle in the variable-area mixing tube are presented in Figs. 3.1-19 through 3.1-22. The theoretical break-off curves are, again, those for an ejector operating under the same conditions but with a constant-area mixing tube of $A_{P1}/A_{MS}$ = 0.516, the area ratio corresponding to the constant-area section of the variable-area tube. As seen in Fig. 3.1-19, the experimental values for $w_S/w_P$ vs $P_{SO}/P_{PO}$ lie very close to the theoretical break-off curve even at low values of $w_S/w_P$. The experimental data for $P_{ATM}/P_{SO}$ vs $P_{PO}/P_{SO}$ as shown in Fig. 3.1-20 indicate that the ejector was operated in the $P_{PO}/P_{ATM}$ independent regime and re-emphasize the undesirability of operation at higher values of $P_{PO}/P_{ATM}$ than required since the mass flow characteristics of Fig. 3.1-19 were identical at each value of $P_{PO}/P_{ATM}$. Figures 3.1-21 and 3.1-22 show that wall pressure variations at low $w_S/w_P$ values were less drastic with the slotted primary

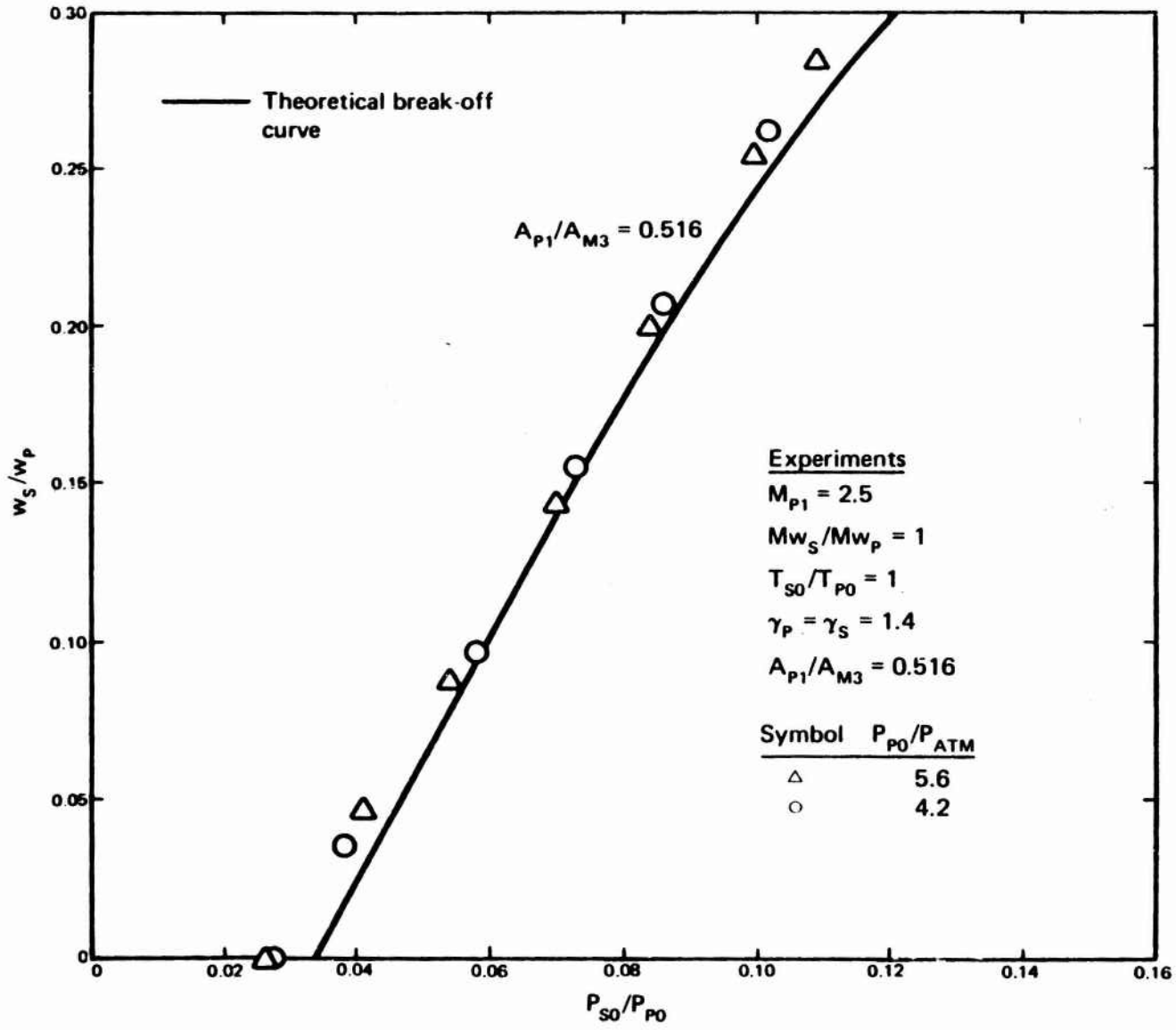


Figure 3.1-19 Variable-area, slotted-nozzle ejector mass flow characteristics ($A_{P1}/A_{M3}$ = 0.516 and $M_{P1}$ = 2.5)

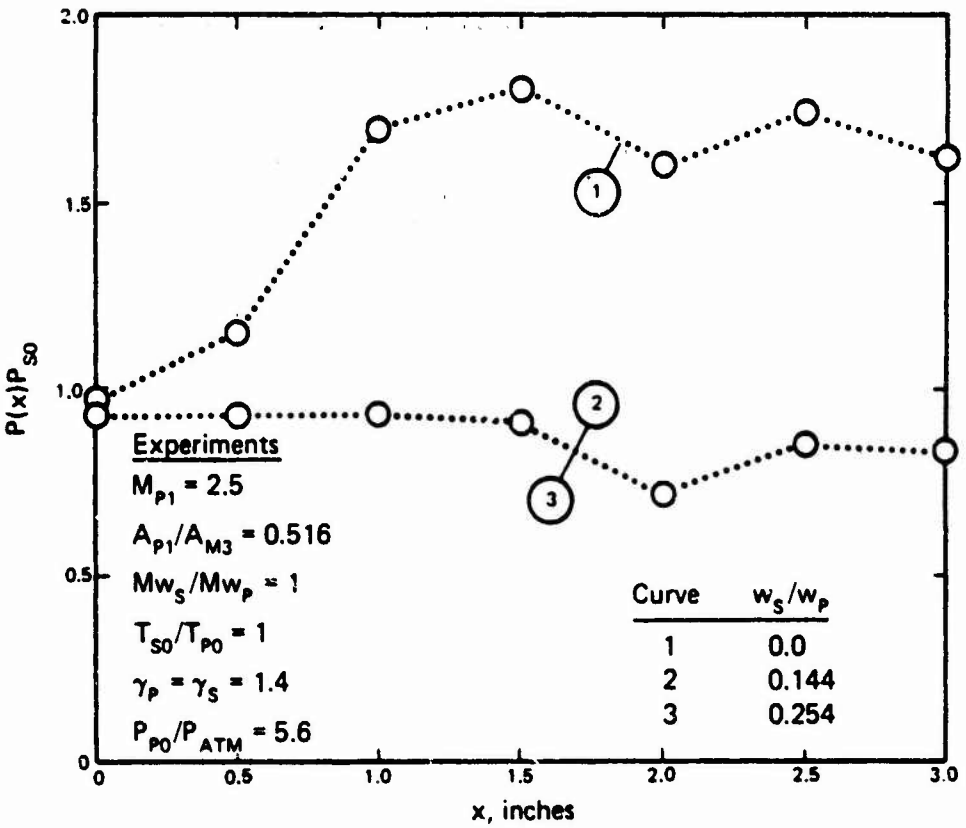


Figure 3.1-21 Variable-area, slotted-nozzle ejector wall pressure distributions ($A_{P1}/A_{M3}$ = 0.516, $M_{P1}$ = 2.5, and $P_{P0}/P_{ATM}$ = 5.6)

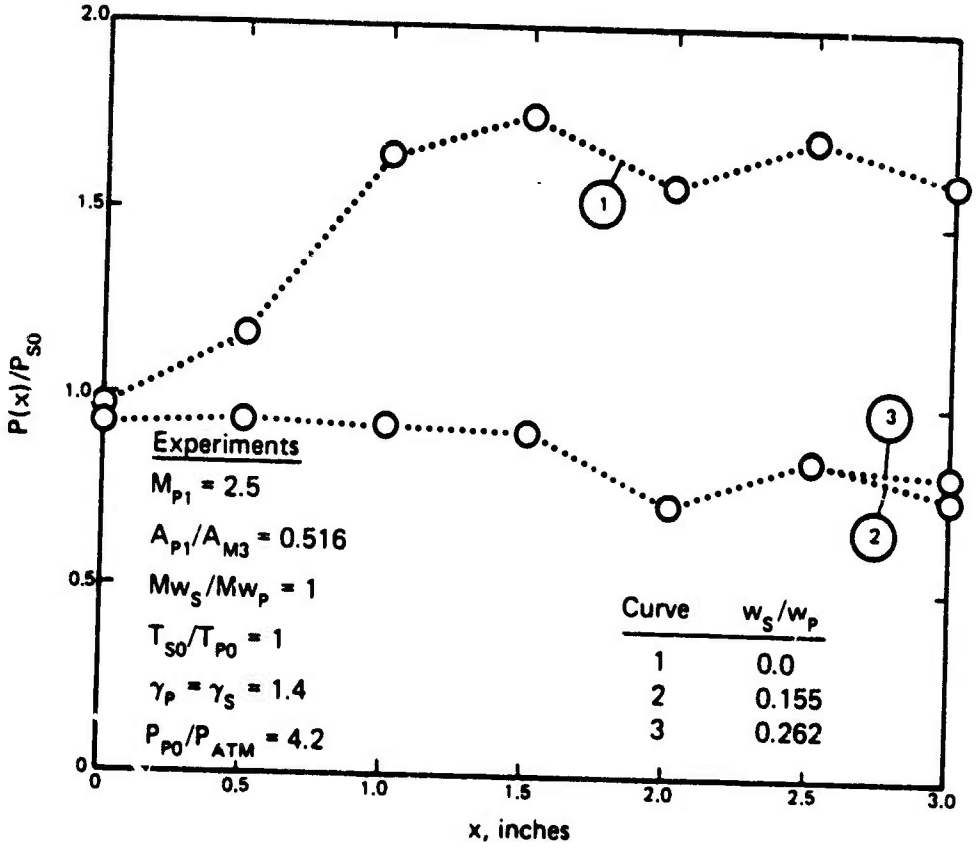


Figure 3.1-22 Variable area, slotted-nozzle ejector wall pressure distributions ($A_{P1}/A_{M3}$ = 0.516, $M_{P1}$ = 2.5, and $P_{P0}/P_{ATM}$ = 4.2)

nozzle as opposed to the conical primary nozzles of Figs. 3.1-15 through 3.1-18 and may account for the excellent agreement of the $w_s/w_p$ vs $P_{so}/P_{po}$ data with the theoretical break-off curve of Fig. 3.1-19, although the constant-area mixing tube data of Fig. 3.1-11 would prejudice any conclusions based on primary nozzle design alone. Again, note that only the initial portions of the wall pressure distributions are presented in Figs. 3.1-21 and 3.1-22.

# 4.0 CONCLUSIONS

Only some general conclusions will be drawn in this section since specific conclusions were included in the foregoing sections. The conclusions are:

(1) The constant-area ejector flow model and computer program should be adopted as the basis for design and system studies. This model most realistically predicts the operational characteristics of ejector systems. The relationship and correspondence between variable-area and constant-area mixing tube ejectors should be established by both experiment and analysis.

(2) The analysis of variable-area mixing-tube ejectors should be continued.

(3) The design of potential high-performance ejector must improve mixing and momentum transfer; some designs with potential are: unsteady flow, periodic pulsating flow, resonance phenomena, and/or various nozzle and mixing-tube geometries.

(4) The computer models developed in this study should be augmented and incorporated into an overall system program and further improvement of sub-system models should be continued.

## 5.0 REFERENCES


1. Addy, A. L., "The Analysis of Supersonic Ejector Systems," Supersonic Ejectors, AGARDograph No. 163, pp. 31-101 (1972).

2. Handbook of Supersonic Aerodynamics, Vol. 6, Section 17, NAVWEPS Report 1488.

3. Fabri, J. and Paulon, J., "Theory and Experiments on Supersonic Air-to-Air Ejectors," NACA TM 1410 (1958).

4. Fabri, J. and Siestrunck, R., "Supersonic Air Ejectors," Advances in Applied Mechanics, New York, New York, Academic Press, Vol. V, pp. 1-34 (1958).

5. Chow, W. L. and Addy, A. L., "Interaction between Primary and Secondary Streams of Supersonic Ejector Systems and their Performance Characteristics," AIAA Journal, 2(4):686-695 (1964).

6. Chow, W. L. and Yeh, P. S., "Characteristics of Supersonic Ejector Systems with Non-Constant Area Shroud," AIAA Journal, 3(3):525-527 (1965).

7. Loth, J. L., "Theoretical Optimization of Staged Ejector Systems," Part I, Arnold Engineering Development Center Report No. AEDC-TR-66-2 (1966).

8. Loth, J. L., "Theoretical Optimization of Staged Ejector Systems," Part II, Arnold Engineering Development Center Report No. AEDC-TR-68-80 (1968).